Received by OSTI
MAY 16 1990

UCID--21702
DE90 010759

Perturbation Growth by Thermal Blooming in Turbulence

T. J. Karr
J. R. Morris
D. H. Chambers
J. A. Viecelli
P. G. Cramer

4 January 1989

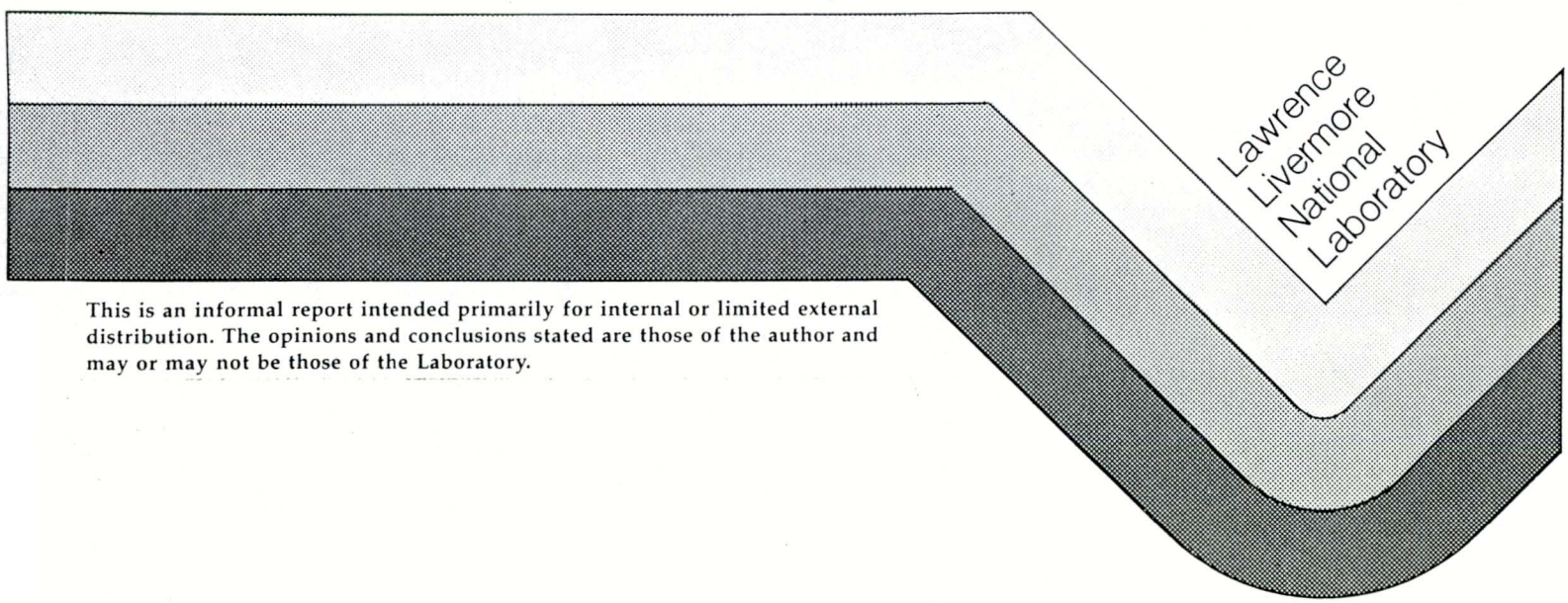

This is an informal report intended primarily for internal or limited external distribution. The opinions and conclusions stated are those of the author and may or may not be those of the Laboratory.

DISTRIBUTION OF THIS DOCUMENT IS UNLIMITED

MASTER

DISCLAIMER

This report was prepared as an account of work sponsored by an agency of the United States Government. Neither the United States Government nor any agency thereof, nor any of their employees, makes any warranty, express or implied, or assumes any legal liability or responsibility for the accuracy, completeness, or usefulness of any information, apparatus, product, or process disclosed, or represents that its use would not infringe privately owned rights. Reference herein to any specific commercial product, process, or service by trade name, trademark, manufacturer, or otherwise does not necessarily constitute or imply its endorsement, recommendation, or favoring by the United States Government or any agency thereof. The views and opinions of authors expressed herein do not necessarily state or reflect those of the United States Government or any agency thereof.

DISCLAIMER

Portions of this document may be illegible in electronic image products. Images are produced from the best available original document.

DISCLAIMER

This document was prepared as an account of work sponsored by an agency of the United States Government. Neither the United States Government nor the University of California nor any of their employees, makes any warranty, express or implied, or assumes any legal liability or responsibility for the accuracy, completeness, or usefulness of any information, apparatus, product, or process disclosed, or represents that its use would not infringe privately owned rights. Reference herein to any specific commercial products, process, or service by trade name, trademark, manufacturer, or otherwise, does not necessarily constitute or imply its endorsement, recommendation, or favoring by the United States Government or the University of California. The views and opinions of authors expressed herein do not necessarily state or reflect those of the United States Government or the University of California, and shall not be used for advertising or product endorsement purposes.

This report has been reproduced
directly from the best available copy.

Available to DOE and DOE contractors from the
Office of Scientific and Technical Information
P.O. Box 62, Oak Ridge, TN 37831
Prices available from (615) 576-8401, FTS 626-8401.

Available to the public from the
National Technical Information Service
U.S. Department of Commerce
5285 Port Royal Rd.,
Springfield, VA 22161

Price Code	Page Range
A01	Microfiche
Papercopy Prices	
A02	001-050
A03	051-100
A04	101-200
A05	201-300
A06	301-400
A07	401-500
A08	501-600
A09	601

PERTURBATION GROWTH BY THERMAL BLOOMING IN TURBULENCE*

T. J. Karr, J. R. Morris, D. H. Chambers,
J. A. Viecelli and P. G. Cramer
Lawrence Livermore National Laboratory
POB 808, L-495
Livermore, CA 94550
(415) 423-6270

4 January 1989

Abstract

The stability of a phase-compensated laser beam propagating in a turbulent absorbing fluid is considered. Small-scale transverse optical perturbations from turbulence and noise grow in thermal blooming by two instabilities: the uncompensated stimulated thermal Rayleigh scattering instability, and the closed-loop instability. Linearized perturbation theory is used to calculate the electric field spectrum as a Taylor series in time and as a superposition of stable and unstable modes. The method is applicable to fluids with arbitrary parameter variations along the path. Compensated perturbations grow exponentially, and uncompensated ones grow quasi-exponentially. The instability growth rates and the turbulence and noise excitation strengths are derived for a simple fluid with homogeneous parameters. The linearized theory of perturbation growth is in good agreement with numerical simulations of full nonlinear thermal blooming. If the growth rate exceeds the damping rate from other phenomena then the perturbations grow until limited by nonlinear saturation, at which point the beam is significantly degraded. At saturation the laser beam spontaneously breaks into small-scale transverse structures such as filaments or ribbons.

*Work performed under the auspices of the U. S. Department of Energy by Lawrence Livermore National Laboratory under contract W-7405-Eng-48, for the U. S. Army in support of funding order No. W31RPD-7-D4041.

The strongest damping mechanism in the open air typically is wind shear, which sets a threshold blooming rate and a threshold absorbed irradiance. Below threshold the perturbations grow linearly, above threshold they grow quasi-exponentially. Other atmospheric damping phenomena such as diffusion and turbulent mixing have a smaller effect.

1. Introduction

A laser beam propagating in an absorbing fluid deposits heat, which consequently changes the fluid's density and refractive index. The induced refractive index changes tend to defocus the beam, a nonlinear phenomenon colorfully known as "thermal blooming." Thermal blooming limits the focusability of an intense laser propagating through the atmosphere.

It is well known that beam perturbations in thermal blooming can grow by the stimulated thermal Rayleigh scattering(STRS) instability[1,2]. Small-scale transverse inhomogeneities of irradiance and phase cause nonuniform heating of the fluid, which produces inhomogeneities of the refractive index. By propagating through these index inhomogeneities, the optical inhomogeneities are amplified in space and time. In very intense beams small fluctuations can grow many orders of magnitude, until either they reach $\mathcal{O}(1)$ and saturate by energy conservation, or they are destroyed by some natural damping mechanism. The STRS instability occurs whether or not optical fluctuations are compensated by an active control system. The growth of fluctuations by STRS on uncompensated or free-running beams has been calculated for initial excitation from noise[1,2] and from thermal turbulence distributed along the path[3] as would be the case in the atmosphere.

If one attempts to actively compensate for optical fluctuations in thermal blooming then a new "closed-loop" instability can occur. There can exist singular modes of the combined system of propagation path-plus-compensation law which have positive feedback to the optical inhomogeneities. These modes grow exponentially in time from an arbitrarily small initial excitation[4-6]. As in the STRS instability, growth continues to saturation at $\mathcal{O}(1)$ unless stopped by some natural damping mechanism. The closed-loop propagation instability is distinct from instabilities of the control loop alone; the closed-loop propagation instability occurs in some "perfect" control loops, e.g. systems which accomplish perfect phase-only correction, and is not a result of imperfect

implementation of the control law. The exponential growth rates have been calculated for several compensation methods[4].

The growth to saturation of small-transverse-scale perturbations in thermal blooming may be the limiting physical process which sets a maximum correctable power for intense laser beams in the atmosphere. Consequently, it is important to predict the saturation point under conditions of concurrent STRS and closed-loop instabilities. This requires detailed knowledge of the space and time evolution of perturbations by thermal blooming. The purpose of this paper is to calculate the perturbation growth of a thermally bloomed laser beam which is partially phase compensated, and calculate in particular the initial excitation and growth from turbulence such as one encounters in the atmosphere.

2. Linearized Theory of Thermal Blooming

Thermal blooming is a locally self-defocusing nonlinear propagation phenomenon. Whole-beam blooming effects are well known and require the full nonlinear description[7,9]. But the appropriate tool for studying instabilities of thermal blooming is the linearized theory of small perturbations. The linearized theory has been presented elsewhere; the reader will find a rigorous discussion in references 4 and 5. Here we mainly state the underlying assumptions and quote without proof the results needed later.

We use the standard model of thermal blooming propagation[7]. The optical electric field $E\exp(i(\omega t - kz))$ obeys the scalar paraxial wave equation,

$$2ik\left(\frac{\partial}{\partial z} + \frac{\alpha_e}{2}\right)E = \nabla^2 E + k^2\left(\frac{\varepsilon}{\varepsilon_0} - 1\right)E \qquad (1)$$

$$\nabla^2 \equiv \frac{\partial^2}{\partial x^2} + \frac{\partial^2}{\partial y^2}$$

where ε is the dielectric constant at frequency ω, $k = 2\pi/\lambda$ is the wavenumber in a uniform fluid of dielectric constant ε_0, and α_e is the extinction coefficient. The beam propagates in the +z direction. This equation is valid for quasimonochromatic light far from the source, propagating in a neutral nonconducting and nonmagnetic fluid[8]. This includes most cases of practical interest, especially laser beams in the atmosphere. The fluid dielectric constant obeys the advection-diffusion equation with isobaric heating,

$$\left(\frac{\partial}{\partial t} + \mathbf{v}\cdot\nabla\right)\varepsilon = -2\varepsilon_0 \mathcal{M}\,\alpha\, I + \mathcal{D}\nabla^2\varepsilon \qquad (2)$$

where $\mathbf{v}(z)$ is the mean transverse fluid velocity, $I = |E|^2$ is the irradiance, α is the absorption coefficient, $\mathcal{M} \equiv \frac{1}{2\varepsilon_0 C_p}\left[\beta_T \frac{\partial \varepsilon}{\partial \rho} - \frac{1}{\rho}\frac{\partial \varepsilon}{\partial T}\right]$ is the fluid thermal response, and $\mathcal{D}$ is the diffusivity. This equation for the fluid is valid as long as (a) the time scale for heating is long compared to the acoustic transit time across the beam, so the fluid is always in pressure equilibrium, and (b) the density changes are too small to affect the velocity field. The optical and fluid fields are nonlinearly coupled by the absorbed irradiance.

The evolution of small-scale or localized perturbations can best be studied by linearizing about a smooth background solution. Choose the background solution to have uniform irradiance I_0 at $z = 0$ and a self-consistent phase ϕ_0, that is $\mathcal{T} I_0$ and ϕ_0 solve Eqs. (1), (2) where $\mathcal{T} = \exp\left(-\int^z \alpha_e\right)$ is the transmission. The electric field envelope with log amplitude and phase fluctuations χ, ϕ around I_0, ϕ_0 is

$$E \equiv \sqrt{\mathcal{T} I_0}\, \exp\left(-i\phi_0 + \chi - i\phi\right) \qquad (3).$$

The small fluctuation μ of the fluid dielectric constant is

$$\mu \equiv \frac{\varepsilon - \varepsilon_0}{2\varepsilon_0}$$

or $$\mu = \frac{n - n_0}{n_0} \quad , \quad n \equiv \sqrt{\varepsilon} \tag{4}.$$

Substituting Eqs.(3), (4) into (1), (2) and retaining only the first order in the perturbations gives[4]

$$\frac{\partial \chi}{\partial z} = -\frac{1}{2k}\nabla^2 \phi \tag{5a}$$

$$\frac{\partial \phi}{\partial z} = k\left(\mu + \frac{1}{2k^2}\nabla^2 \chi\right) \tag{5b}$$

$$\left(\frac{\partial}{\partial t} + \mathbf{v} \cdot \nabla\right)\mu = -2\Gamma\chi + \mathscr{D}\nabla^2\mu \tag{6}$$

where $\Gamma = \mathscr{M}\alpha\mathscr{T}I_0$. The equations are Fourier transformed in the transverse xy plane and Laplace transformed in time to obtain

$$\frac{\partial \hat{\chi}}{\partial z} = a_\kappa \hat{\phi} \tag{7a}$$

$$\frac{\partial \hat{\phi}}{\partial z} = k\hat{\mu} - a_\kappa \hat{\chi} \tag{7b}$$

$$\left(\nu + \mathscr{D}\kappa^2 - i\kappa \cdot \mathbf{v}\right)\hat{\mu} = -2\Gamma\hat{\chi} + \mu^0 \tag{8}$$

where κ is the transverse wavevector, all fields (χ, ϕ and μ) are Fourier amplitudes at κ, $a_\kappa = \kappa^2/2k$, ν is the complex Laplace variable conjugate to time, caret ^ indicates Laplace transform, and μ^0 is the t = 0 refractive index perturbation. Eqs. (7) and (8) can be combined into a second order equation for the irradiance fluctuation $F = 2\chi$:

$$\frac{d^2 \hat{F}}{dz^2} + a_\kappa^2 \beta^2 \hat{F} = \frac{2a_\kappa k \mu^o}{\bar{\nu}} \qquad (9)$$

where $\beta^2(z, \nu) \equiv 1 + \frac{2k\Gamma(z)}{a_\kappa \bar{\nu}(z)}$, $\bar{\nu}(z) \equiv \nu + \mathcal{D}(z)\kappa^2 - i\kappa \cdot \mathbf{v}(z)$,

and $\frac{d\hat{F}}{dz} = 2a_\kappa \hat{\phi}$. Eqs. (7) - (9) determine the growth (or decay) of the perturbation as a function of z and t.

Perturbation solutions are completely determined by the boundary conditions, which are the optical fields χ, ϕ (or equivalently F, dF/dz) at z = 0 and the refractive index field μ^0 at t = 0. The perturbations at z > 0, t > 0 are given by four Green functions, denoted J, K, L and b, integrated over the boundary conditions. We write the solution in a compact "vector" notation. Intensity and phase perturbations are grouped into 2 x 1 vectors with i- and ϕ-components: $\mathbf{F} \equiv (F, dF/dz)$ and $\mu \equiv (0, \mu)$. The Green functions are 2x2 matrices of operators with matrix elements labeled ii, iϕ, etc. [We sometimes use the same letter to represent the operator matrix and its iϕ matrix element; the meaning is always clear from the context.] The solution is [4,5]

$$\hat{\mathbf{F}}(z) = \hat{\mathbf{J}}(z|0)\hat{\mathbf{F}}(0) + \kappa^2 \int_0^z \hat{\mathbf{K}}(z|s)\mu^0(s)\,ds \qquad (10)$$

$$\kappa^2 \hat{\mu}(z) = -\hat{\mathbf{b}}(z)\hat{\mathbf{J}}(z|0)\hat{\mathbf{F}}(0) + \kappa^2 \int_0^z \hat{\mathbf{L}}(z|s)\mu^0(s)\,ds \qquad (11).$$

The subscript κ has been dropped since all subsequent analysis will be in the Fourier domain. Green function $\hat{\mathbf{J}}$ is the homogeneous solution of Eq. (9), that is it obeys

$$\frac{d\hat{\mathbf{J}}(z|s)}{dz} + \begin{pmatrix} 0 & -1 \\ a_k^2\beta^2(z) & 0 \end{pmatrix} \hat{\mathbf{J}}(z|s) = 0$$

with the boundary condition

$$\hat{\mathbf{J}}(s|s) = \begin{pmatrix} 1 & 0 \\ 0 & 1 \end{pmatrix} .$$

All other Green functions are constructed from β and $\hat{\mathbf{J}}$:

$$\hat{\mathbf{K}}(z|s) = \frac{\hat{\mathbf{J}}(z|s)}{\bar{v}(s)} ,$$

$$\hat{\mathbf{b}} = \begin{pmatrix} 0 & 0 \\ a_\kappa^2[\beta^2 - 1] & 0 \end{pmatrix} ,$$

and $\hat{\mathbf{L}}(z|s) = -\hat{\mathbf{b}}(z)\,\hat{\mathbf{K}}(z|s) + \frac{\delta(z-s)}{\bar{v}(s)}$.

$\mathbf{J}$ is the source Green function; its unstable growth in z and t is well known, and is due to stimulated thermal Rayleigh scattering (STRS)[1-3]. $\mathbf{K}$ is the turbulence-blooming interaction Green function; it describes the rapid growth by blooming of perturbations induced by refractive index turbulence[3].

The Green functions at t = 0, and at all time without thermal blooming, are

$$\mathbf{K}^\circ(z|0) = \exp(i\kappa \cdot \mathbf{v}t - \mathcal{D}\kappa^2 t) \begin{pmatrix} \cos a_\kappa z & \frac{1}{a_\kappa} \sin a_\kappa z \\ -a_\kappa \sin a_\kappa z & \cos a_\kappa z \end{pmatrix}$$

$$\mathbf{L}^\circ(z|0) = \exp(i\kappa \cdot \mathbf{v}t - \mathcal{D}\kappa^2 t)\ \delta(z)$$

and $\mathbf{J}^\circ(z|0) = \mathbf{K}^\circ(z)\ \delta(t)$.

With these Green functions one can derive all the standard results of the classical theory of propagation through weak turbulence [11,12].

Systems with optical compensation have two beams, an "intense" laser beam originating at z = 0 and propagating in the +z direction which induces refractive index changes by absorption, and a reference "beacon" beam originating at z = L and propagating in the -z direction which is affected by the refractive index but which is too weak to induce significant index change of its own. The beacon enables one to observe propagation conditions of the intense beam path with a sensor at the intense beam transmitter (z = 0). This is known as "return wave sensing". The beacon perturbation solution vector $\mathbf{F}^b \equiv (F^b, -dF^b/dz)$, given the additional boundary conditions of $\mathbf{F}^b$ at z = L, is[4,5]

$$\hat{\mathbf{F}}^b(z) = \hat{\mathbf{J}}^b(L - z)\hat{\mathbf{F}}^b(L) - \hat{\mathbf{B}}(L|z)\hat{\mathbf{F}}(z) + \kappa^2 \int_z^L \hat{\mathbf{J}}^b(s - z) \int_0^s \hat{\mathbf{L}}(s|r)\mu^o(r)\, d\, r\, d\, s \qquad (12).$$

$\mathbf{J}^b$ is the beacon Green function without blooming, i.e. the homogeneous solution of Eq. (9) for $\Gamma = 0$ with beacon wavenumber k_b; it is space-invariant and therefore acts as a correlation kernel. The beacon-blooming Green function

$$\hat{\mathbf{B}}(L|z) \equiv \int_z^L \hat{\mathbf{J}}^b(s - z)\hat{\mathbf{b}}(s)\hat{\mathbf{J}}(s|z)\, d\, s \qquad (13)$$

gives the beacon effect on intense-beam perturbations. Green function $\mathbf{b}(z)$ is the infinitesimal version of Green function $\mathbf{B}(L|z)$. The complete solution in terms of the boundary conditions and five Green functions is shown in Fig. 1.

A correction system creates an intense beam perturbation at z = 0 based on a measurement of the beacon perturbation at z = 0. The intense beam produced by a linear real-time control process is

$$\hat{\mathbf{F}}(0) = \hat{\mathbf{G}}\hat{\mathbf{F}}^b(0) + \hat{\mathbf{f}} \qquad (14)$$

where **G** is a 2x2 matrix representing the control law and **f** is noise. In general **G** can mix perturbations at different transverse wavevectors, although we will usually discuss

the simpler case of **G** diagonal in κ. the beacon solution Eq.(12) into the linear control process Eq. (14) gives the intense field at z = 0:

$$\hat{\mathbf{F}}(0) = \left[\mathbf{1} + \hat{\mathbf{G}}\,\hat{\mathbf{B}}(L|0)\right]^{-1}\hat{\mathbf{G}}\left(\hat{\mathbf{J}}^{b}(L)\,\hat{\mathbf{F}}^{b}(L) + \kappa^{2}\int_{0}^{L}\hat{\mathbf{J}}^{b}(s)\int_{0}^{s}\hat{\mathbf{L}}(s|r)\,\mu^{0}(r)\,dr\,ds\right) + \left[\mathbf{1} + \hat{\mathbf{G}}\,\hat{\mathbf{B}}(L|0)\right]^{-1}\hat{\mathbf{f}} \quad (15).$$

The intense field anywhere else along the path is found by substituting this into the propagating solution, Eq.(10).

If the operator $\mathbf{1} + \hat{\mathbf{G}}\,\hat{\mathbf{B}}$ is singular, i.e. if

$$\det\left(\mathbf{1} + \hat{\mathbf{G}}\,\hat{\mathbf{B}}\right) \equiv \Delta = 0 \quad (16),$$

then the result of the correction system is *unstable* in thermal blooming. This is known as the closed-loop instability[4]. It is an absolute instability. Control laws generally are unstable in blooming; stable control laws are the exception. Eq. (16) is a transcendental equation for the dispersion relation $\nu(\kappa)$ of the instability.

A common method of optical compensation is phase reversal (also called phase-only or phase-conjugate correction)--the intense beam is launched with an optical path difference (OPD) which is the opposite of that on the beacon. This is implemented by real-time adaptive optics[10]. The sensing and correction typically is done on a two-dimensional lattice of points, which is space-variant, so generally the control system mixes spatial frequencies (the G operator in Eq. (14) is not diagonal in κ-space). For simplicity we start with an idealized space-invariant model of the adaptive optics which is diagonal in κ (in a later section we discuss how this is extended to a more complete description of adaptive optics). The control law matrix for this idealized phase-only correction is

$$\hat{\mathbf{G}} = \begin{pmatrix} 0 & 0 \\ 0 & -g(\kappa, \nu) \end{pmatrix} \quad (17)$$

where g is the control loop gain (perfect correction = 1), and the propagator is

$$\left[\mathbf{1} + \hat{\mathbf{G}}\,\hat{\mathbf{B}}\right]^{-1} = \begin{pmatrix} 1 & 0 \\ \dfrac{g\,\hat{B}_{\varphi i}}{\Delta} & \dfrac{1}{\Delta} \end{pmatrix} \tag{18}.$$

In this case $\Delta = 1 - g\,\hat{B}_{\varphi\varphi}$. The singular behavior of this propagator in thermal blooming is known as the "phase compensation instability" or PCI.

The various thermal blooming Green functions can be written in closed form for only a few cases of heating $\Gamma(z)$ and flow velocity $\mathbf{v}(z)$.

However, for $\left|\dfrac{d\beta}{dz}\Big/ a_\kappa \beta^2\right| << 1$ a WKB approximation to $\hat{\mathbf{J}}$ can be obtained [4]:

$$\hat{J}_{i\varphi}(z|s) = \frac{1}{a_\kappa \sqrt{\beta(z)\,\beta(s)}} \sin a_\kappa \int_s^z \beta \tag{19}.$$

The special case of uniform $\mathcal{D}$, v and Γ can be solved in closed form[4]. We study this case in detail in the next sections. Note that uniform diffusion simply gives a multiplicative factor of $\exp(-\mathcal{D}\kappa^2 t)$ on all Green functions. If velocity is uniform, i.e. $\mathbf{v}(z) = v$, the $i\boldsymbol{\kappa}\cdot\mathbf{v}$ term in Eq.(8) can be eliminated by transforming to the convected frame, $x \rightarrow x - vt$. With these simplifications, the intense beam Green functions in the complex plane are

$$\hat{\mathbf{J}}(z) = \bar{v}\,\hat{\mathbf{K}}(z) = \begin{pmatrix} \cos a_\kappa \beta z & \dfrac{1}{a_\kappa \beta} \sin a_\kappa \beta z \\ -a_\kappa \beta \sin a_\kappa \beta z & \cos a_k \beta z \end{pmatrix} \tag{20}.$$

In the convected frame time domain, the Green functions ($i\varphi$ matrix element) neglecting diffusion are

$$K(z,t) = \sum_{n=0}^{\infty} \frac{(-\Gamma kzt)^n}{(n!)^2} [z\, j_n(a_\kappa z)] \tag{21a}$$

$$\text{and } J(z,t) = \frac{\partial}{\partial t} K(z,t) + K(z,0)\,\delta(t) \tag{21b}.$$

Here j_n is the spherical Bessel function of the first kind, and Γkzt is the radians of phase shift due to heating for time t. The beacon-blooming Green functions we will use later are

$$\hat{B}_{\varphi\varphi} = \frac{\beta^2 - 1}{\beta^2 - b^2}\left[1 - \cos\beta\ell\,\cos b\ell - \frac{b}{\beta}\sin\beta\ell\,\sin b\ell\right] \tag{22a}$$

$$\hat{B}_{\varphi i} = a_\kappa^b \frac{\beta^2 - 1}{\beta^2 - b^2}\left[\frac{\beta}{b}\sin\beta\ell\cos b\ell - \cos\beta\ell\sin b\ell\right] \tag{22b}$$

where $\ell \equiv a_\kappa L$ is a dimensionless measure of the optical path length and the transverse wavenumber κ, and $b \equiv k/k_b$ (no relation to blooming operator $\hat{\mathbf{b}}$ below Eq. (11)).

3. Closed-Loop Green Function of Thermal Blooming

For the uniform fluid the closed-loop Green function for phase-only correction (PC) can be written in closed form. The turbulent and absorbing fluid extends from z = 0 to z = L, the beacon is an infinite plane wave at z = L ($\mathbf{F}^b = 0$), and the intense field at z = 0 has phase noise ψ and log amplitude noise η. Substituting Eqs.(22) and (18) into (15) gives the field at z = 0:

$$\hat{F}(0) = 2\hat{\eta} \tag{23a}$$

$$\hat{F}'(0) = 2a_\kappa \hat{\phi}(0) = \frac{1}{\Delta}\left[\frac{\kappa^2}{k}\hat{\psi} + 2g\,\hat{B}_{\varphi i}\hat{\eta}\right] - \frac{1}{\bar{\nu}}\int_0^L \hat{M}(s)\,\kappa^2\,\mu^0(s)\,ds \tag{23b}$$

where prime ′ indicates d/dz, and $\widehat{M}/\bar{\nu}$ is the control system response to index fluctuations at range s,

$$\widehat{M}(s) \equiv \frac{g}{\Delta}\left\{\frac{\beta^2 - 1}{\beta^2 - b^2}[1 - \cos ba_\kappa s] + \cos ba_\kappa s - Q(s)\right\} \tag{24}$$

with $Q(s) \equiv \dfrac{\beta^2 - 1}{\beta^2 - b^2}\left[1 - \cos \beta a_\kappa (L - s)\cos ba_\kappa L - \dfrac{b}{\beta}\sin \beta a_\kappa (L - s)\sin ba_\kappa L\right]$.

Note that $\Delta = 1 - gQ(0)$. The field, Eq.(23), is a function only of the noise and the initial refractive index.

The log amplitude and phase of the intense field at z is

$$\begin{aligned}\widehat{\chi}(z) = {} & a_\kappa k \int_0^z \widehat{K}(z - s)\mu^0(s)\,ds - a_\kappa k \widehat{K}(z)\int_0^L \widehat{M}(s)\mu^0(s)\,ds \\ & + \bar{\nu}\widehat{K}'(z)\widehat{\eta} + \bar{\nu}a_\kappa \widehat{K}(z)\frac{1}{\Delta}\left[\widehat{\psi} + \frac{g\widehat{\eta}\widehat{B}_{\varphi i}}{a_\kappa}\right]\end{aligned} \tag{25}$$

$$\begin{aligned}\widehat{\phi}(z) = {} & k\int_0^z \widehat{K}'(z - s)\mu^0(s)\,ds - k\widehat{K}'(z)\int_0^L \widehat{M}(s)\mu^0(s)\,ds \\ & + \frac{\bar{\nu}}{a_\kappa}\widehat{K}''(z)\widehat{\eta} + \bar{\nu}\widehat{K}'(z)\frac{1}{\Delta}\left[\widehat{\psi} + \frac{g\widehat{\eta}\widehat{B}_{\varphi i}}{a_\kappa}\right]\end{aligned} \tag{26}$$

where K denotes the iφ matrix element. By inspection of Eqs.(25), (26) the closed-loop turbulence-blooming Green function for phase-only correction is

$$\widehat{K}^{PC}(z|s) = \widehat{K}(z)\widehat{M}(s) \tag{27}.$$

The effect of turbulence on the optical field is

$$\hat{F}(z) = \kappa^2 \int_0^z \hat{K}(z-s)\,\mu^0(s) - \kappa^2 \int_0^L \hat{K}^{PC}(z|s)\,\mu^0(s)\,ds \qquad (28).$$

$$+ \text{ noise}$$

If we expand the Green functions to $\mathcal{O}(\nu^{-n})$ and Laplace invert term-by-term, we get the Green functions as Taylor series in time. The Taylor series are absolutely convergent for all $t > 0$. For the special case of g independent of ν (which corresponds to a control loop with instantaneous feedback and infinite bandwidth) and b=1, the time-dependent PC Green function without diffusion ($i\varphi$ matrix element) is

$$K^{PC}(z|s,t) = \frac{g}{2a_\kappa} \sum_{n=0}^{\infty} \frac{(2\Gamma kt/a_\kappa)^n}{n!} \sum_{m=0}^{n} \frac{(-1)^m T_{n-m}(u)}{2^m\, m!\,(n-m)!} \qquad (29a)$$

$$\cdot \left\{\cos u\left[(2u-w)^{m+1} j_m(2u-w) + w^{m+1} j_m(w)\right]\right.$$

$$\left. + \frac{\sin u}{2^{m+1}}\left[(2u-w)^{m+2} \sum_{l=0}^{m} \binom{m}{l} j_l\left(u-\frac{w}{2}\right) j_{m-l}\left(u-\frac{w}{2}\right) - w^{m+2} \sum_{l=0}^{m} \binom{m}{l} j_l\left(\frac{w}{2}\right) j_{m-l}\left(\frac{w}{2}\right)\right]\right\}$$

where $u = a_\kappa z$, $w = a_\kappa s$, and

$$T_0(u) = 1,\ T_n(u) = -gu \sum_{l=0}^{n-1} \left(\frac{-u}{2}\right)^{n-l} \binom{n}{l} T_l(u)\left[\sin u\, j_{n-l}(u) + \cos u\, j_{n-l-1}(u)\right] \qquad (29b).$$

This should be compared to the free-running Green function, Eq.(21).

4. Growth of Turbulence-Induced Perturbations

Of great practical interest is the interaction between blooming and a random field of initial refractive index perturbations. In this case the appropriate measures of optical perturbations are the *spectra* of log amplitude and phase. For a uniform fluid these are

$$\begin{aligned}\langle \chi \chi^{*}(z,t)\rangle \;=\; a_\kappa^2 k^2 \Bigg\{ & \int_0^z \int_0^z K(z-s,t)\,K(z-s',t)\,\langle \mu^0(s)\,\mu^{0*}(s')\rangle\, ds\, ds' \\ & + \int_0^L \int_0^L K^{PC}(z|s,t)\,K^{PC}(z|s',t)\,\langle \mu^0(s)\,\mu^{0*}(s')\rangle\, ds\, ds' \\ & - 2\int_0^z \int_0^L K(z-s;t)\,K^{PC}(z|s',t)\,\mathrm{Re}\,\langle \mu^0(s)\,\mu^{0*}(s')\rangle\, ds\, ds' \Bigg\}\end{aligned} \tag{30a}$$

$$\begin{aligned}\langle \phi\phi^{*}(z,t)\rangle \;=\; k^2 \Bigg\{ & \int_0^z \int_0^z K'(z-s,t)\,K'(z-s',t)\,\langle \mu^0(s)\,\mu^{0*}(s')\rangle\, ds\, ds' \\ & + \int_0^L \int_0^L K^{PC'}(z|s,t)\,K^{PC'}(z|s',t)\,\langle \mu^0(s)\,\mu^{0*}(s')\rangle\, ds\, ds' \\ & - 2\int_0^z \int_0^L K'(z-s,t)\,K^{PC'}(z|s',t)\,\mathrm{Re}\,\langle \mu^0(s)\,\mu^{0*}(s')\rangle\, ds\, ds' \Bigg\}\end{aligned} \tag{30b}$$

where brackets <> indicate an ensemble average over realizations of the random field.

In the special case of locally homogeneous thermal turbulence, the index fluctuations have a Kolmogorov spectrum with amplitude characterized by the structure constant $C_\mu^2(z)$, which is generally a function of position along the path. Following Tatarskii[11], the spectra are given by

$$\langle \chi\chi^{*}(L,t)\rangle \simeq a_{\kappa}^{2}k^{2}\cdot 2\pi\Phi^{0}\int_{0}^{L} C_{\mu}^{2}(s)\left[K(L-s,t)-K^{PC}(L|s,t)\right]^{2} ds \qquad (31a)$$

$$\langle \phi\phi^{*}(L,t)\rangle \simeq k^{2}\cdot 2\pi\Phi^{0}\int_{0}^{L} C_{\mu}^{2}(s)\left[K'(L-s,t)-K^{PC'}(L|s;t)\right]^{2} ds \qquad (31b)$$

where $$\int_{-\infty}^{\infty}\langle \mu^{0}(s)\,\mu^{0*}(s+\zeta)\rangle\, d\zeta = 2\pi\Phi^{0}C_{\mu}^{2}(s) \qquad (32)$$

is the spectrum of initial turbulent index fluctuations, and Φ^{0} is the fundamental Kolmogorov spectrum of a passive contaminant[11,12]

$$\Phi^{0} = \frac{.033}{\kappa^{11/3}} \qquad (33).$$

The transverse coherence length r_0 of the turbulence is defined as

$$r_{o} \equiv \left[(0.423)\,k^{2}\int_{0}^{L} C_{\mu}^{2}(s)\,ds\right]^{-3/5} .$$

The end-of-path electric field spectrum $\Phi \equiv \langle |E_{\kappa}|^{2}\rangle$. In the linearized theory the field spectrum is equal to the sum of the log amplitude and phase spectra or variance $\Phi \simeq \langle\chi\chi\rangle^{*} + \langle\phi\phi\rangle^{*}$, since these variances are small and the higher-order correlations can be neglected. We will use the term "field spectrum" interchangebly with the "sum of the variances of χ and ϕ", except in situations where the field perturbation becomes large and the premises of linearized theory are violated.

The field spectrum has three parts: open loop (~K^2), closed loop (~K^{PC2}) and mixed (~KK^{PC}). Each part is a Taylor series in time, and the nth term is rather lengthy to write. The Appendix contains the general formula of the field spectrum for uniform

initial turbulence $\left(C_\mu^2 \text{ independent of } z\right)$. Here we make some general observations and numerically evaluate an example.

In the linearized blooming theory the optical spectrum induced by turbulence always is proportional to the initial index spectrum, as in Eq. (31). This is a direct consequence of linearity, and holds for any profile $\Gamma(z)$ and $\mathbf{v}(z)$. For initially uniform turbulence the spectrum Φ is proportional to $N_T^{-5/6}$, where

$$N_T \equiv \frac{k r_0^2}{8L} = \frac{\pi r_0^2}{4\lambda L}$$

is the turbulence Fresnel number. In a uniform fluid the appropriate measure of transverse wavenumber κ and of path length L is the dimensionless quantity $\ell \equiv a_\kappa L$ or equivalently the Fresnel number N_p of the perturbation,

$$N_p \equiv \frac{\pi^2 k}{2\kappa^2 L} = \frac{\pi^2}{4\ell} \quad .$$

The appropriate measure of time is the phase shift, due to heating of the fluid by the uniform background beam for time t, in "radians of blooming" $\theta \equiv \Gamma k z t$ or equivalently "waves of blooming" N_λ,

$$N_\lambda \equiv \frac{\Gamma k z t}{2\pi} \quad .$$

The initial spectrum with an instantaneous PC feedback loop is

$$\Phi(t = 0) = \frac{.0243\, L}{k\, N_T^{5/6}\, \ell^{11/6}} \left[1 + \frac{1}{2}\left(g^2(\ell) - 2g(\ell)\right)\left(1 + \frac{\sin 2\ell}{2\ell}\right)\right] \qquad (34).$$

If a wavenumber κ is perfectly phase corrected ($g(\kappa) = 1$) then Eq.(34) means the initial end-of-path spectrum contains only the scintillation of uncorrected turbulence at κ; the turbulent phase fluctuations at κ are completely eliminated. At $t > 0$ (or $N_\lambda > 0$) phase and log amplitude fluctuations grow by STRS and PCI.

Fig. 2 is an example. The optical spectrum Φ is calculated for a path with uniform Γ, v and $\mathcal{D}$. The limited spatial resolution of a PC control loop is modeled by a

wavenumber cutoff κ_{PC} or equivalently a Fresnel number cutoff N_{PC}; perturbations with $N_P > N_{PC}$ get some phase correction, while $N_P < N_{PC}$ are uncorrected. Initially Φ contains mainly scintillation below cutoff and is Kolmogorov above cutoff. After blooming the spectrum below loop cutoff shows PCI exponential growth, with the shortest wavelengths growing the fastest; the spectrum above cutoff shows STRS growth.[3] Whether the spectral growth is fastest for controlled perturbations or uncontrolled perturbations, i.e. whether PCI or STRS dominates, depends on the choice of control loop cutoff N_{PC}.

The wave structure function[12] is

$$D(r, \theta) = 4\pi \frac{k}{L} \int_0^\infty \Phi(\ell, \theta) \left[1 - J_0\left(r \sqrt{2k/L}\, \sqrt{\ell}\right)\right] d\ell \qquad (35)$$

where J_0 is a Bessel function. Fig. 3 shows the structure function for this example. The Strehl ratio may be calculated in general by an aperture average of the mutual coherence function $\exp\left(-\frac{1}{2} D\right)$, or in linearized theory simply by summing the energy $\mathcal{E}^*$ in all perturbations,

$$\text{Strehl} \approx 1 - \mathcal{E}^* \equiv 1 - \int\int \Phi \, d\kappa_x \, d\kappa_y \qquad (36),$$

$$= 1 - 2\pi \frac{k}{L} \int_0^\infty \Phi(\ell, \theta) \, d\ell \qquad \text{(isotropic)}$$

so long as $\mathcal{E}^*$ is finite (as is the case for perfect phase correction at long wavelengths). Both methods give the same result in linearized theory.

5. Decomposition Into Singular Modes

The representation of the PC Green function and wave spectrum as Taylor series in time (Eqs.(29) and (A9) - (A11)) is convenient, but it does not give much physical insight. In each order many different growth phenomena with different rates are superimposed and beat together. In this section we clarify the physics by representing the optical field as a superposition of modes. Each mode has a direct physical

interpretation. Both growing and damped modes are present. In general an infinite number of modes are required at each spatial frequency, which is not very tidy. But every spatial frequency usually has a single dominant mode, so a simple physical description explains the thermal blooming phenomenology. Our analysis is for phase-only correction in an atmosphere of uniform Γ, v and $\mathcal{D}$, but the method is generalizable to other control laws and atmospheres.

Consider the intense field fluctuation $\hat{\mathbf{F}}(0)$ created by the control system in response to thermal blooming, Eq. (23). The response operator $\hat{\mathbf{M}}$ has the following singularity structure in the complex ν–plane (Fig. 4): (a) an infinite number of poles at zeros of Δ, (b) an essential singularity at $-\mathcal{D}\kappa^2$ which also is an accumulation point of poles, (c) poles in g/Δ at the finite resonances of the control system under load, and (d) a singularity at ∞, $\hat{\mathbf{M}}(s, \nu \to \infty) = g(\kappa, \nu \to \infty) \cos ba_\kappa s$. The noise contribution to $\hat{\mathbf{F}}(0)$ has the same singularities. Call ν_1 the zero of Δ with largest real part; number the other zeros ν_j in the order of decreasing real part. Call ν_{-1} the pole of g/Δ with largest negative real part; number the other poles ν_{-j} in the order of decreasing real part. Number the residues Res_j in the same way.

For every singularity there is a unique spatiotemporal mode. If the spatial distribution of index $\mu^0(s)$ has nonzero overlap on $\mathrm{Res}_j(s)$ then the jth mode is excited. Also, if the noise $\hat{\mathbf{f}}(\nu_j) \neq 0$ then the jth mode is excited. Modes with Re $\nu_j > 0$ grow, modes with Re $\nu_j < 0$ decay. In the absence of blooming $\Gamma = 0$ and $\Delta = 1$, the properly designed control system has all the poles of g in the left half-plane, and all modes decay--i.e. the control system damps all fluctuations. This of course is what we expect from a feedback control loop. However, with blooming there also are growing modes(in fact an infinite number of them if one neglects diffusion)which are excited by the random index field and by noise. With blooming the same control system does not damp all fluctuations, but must amplify some of them.

All the spatiotemporal structure of the modes, and the decomposition of the intense field at any point into its constituent modes, can be found by the following analysis(which we only sketch here).

1. Invert $\widehat{M}(\nu) \rightarrow M(t)$ by Mellin transform. One can show that at $t > 0$

$$M(s, t) = \sum_j \exp(\nu_j t)\, \mathrm{Res}_j(s) + g(\infty)\, \delta(t) \cos b a_\kappa s \qquad (37),$$

where the infinite sum is absolutely convergent ($\mathrm{Res}_n \sim 1/n^2$) and the essential singularity does not contribute.

2. Laplace transform $M(t) \rightarrow \widehat{M}(\nu)$ to obtain

$$\widehat{M}(s, \nu) = \sum_j \frac{\mathrm{Res}_j(s)}{\nu - \nu_j} + g(\infty) \cos b a_\kappa s \qquad (38).$$

3. Rearrange $\widehat{M}/\bar{\nu}$ as a sum of poles with

$$\frac{1}{\bar{\nu}(\nu - \nu_j)} = \frac{1}{\nu_j^0(\nu - \nu_j)} - \frac{1}{\bar{\nu}\, \nu_j^0} \qquad (39)$$

where $\nu_j^0 = \nu_j + \mathcal{D}\kappa^2$.

4. Substitute Eqs. (38), (39) into (25), (26) to obtain the optical perturbations on the intense beam at z. Each pole term combines with $\widehat{\mathbf{J}}(z)$, Eq. (20). This gives the propagated mode an essential singularity at $-\mathcal{D}\kappa^2$ from $\beta(\bar{\nu})$, in addition to the pole at ν_j. The jth mode has two parts: a part like $\exp(\nu_j t)\, \widehat{\mathbf{J}}(z, \nu_j)$ that *grows* (or decays) *exponentially*, and a subexponential part from the essential singularity.

5. The jth mode has a multiplicative index source

$$S_j = \int_0^L \mu''(s) \frac{\mathrm{Res}_j(s)}{\nu_j^0}\, ds \qquad (40a)$$

and noise source

$$N_j = \mathrm{Res}\left(\frac{1}{\Delta_j}\right) \frac{\widehat{\psi}_j}{k} + \mathrm{Res}\left(\frac{g_j}{\Delta_j}\right) \frac{\left(\widehat{\eta}\, \widehat{B}_{\varphi i}\right)_j}{k\, a_\kappa} \qquad (41)$$

where subscript j indicates a quantity evaluated at $\nu = \nu_j$. The singularities at $-\mathcal{D}\kappa^2$ and ∞ also have index sources

$$S_{\substack{o \\ \infty}} = \int_0^L \mu^o(s) \begin{Bmatrix} \widehat{M}\left(s, \nu = -\mathcal{D}\kappa^2\right) \\ g(\infty) \cos ba_\kappa s \end{Bmatrix} ds \qquad (40b).$$

The limit $\nu \to -\mathcal{D}\kappa^2$ is taken along any contour that avoids all the poles.

With blooming $S_o = 0$. With real control loops $g(\infty) = S_\infty = 0$.

6. The sources obey a sum rule,

$$\sum_{j \neq 0} S_j = S_\infty - S_o \qquad (= 0 \text{ usually}) \qquad (42)$$

$$\sum_j N_j = 0 \qquad (43).$$

Note that

$$\sum_{j \neq 0} S_j = \lim_{\varepsilon \to 0} \int_0^L ds\, \mu^0(s) \left\{ \frac{1}{2\pi i} \int d\nu \frac{\widehat{M}(s, \nu) - \widehat{M}(s, \infty)}{\nu - \varepsilon} - \left[\widehat{M}(s, -\mathcal{D}\kappa^2) - \widehat{M}(s, \infty) \right] \right\}$$

where the contour encloses all the poles and the limit $\varepsilon \to 0$ avoids the poles. But this $\int = 0$, which proves Eq.(42).

7. For ν_j a first-order zero of Δ, the sources are

$$S_j = \int_0^L ds\, \mu^0(s) \frac{g_j}{\nu_j^0 \dfrac{\partial \Delta}{\partial \nu_j}} \left\{ \frac{\beta^2 - 1}{\beta^2 - b^2} \left[1 - \cos ba_\kappa s \right] + \cos ba_\kappa s - Q(s) \right\}_j \qquad (44)$$

$$N_j = \frac{\nu_j}{\nu_j \dfrac{\partial \Delta}{\partial \nu_j}} \frac{1}{k} \left[\widehat{\psi} + g\eta \frac{\widehat{B}_{\varphi i}}{a_\kappa} \right]_j \qquad (45).$$

8. The essential singularity also contains the open-loop or free-running STRS contribution from the index field and the noise. We call this the zeroth mode.

By this analysis one obtains the intense optical field perturbation as a

superposition of the modes:

$$F(z,t) = 2\chi(z,t) =$$

$$K(\bullet,t) * \kappa^2 \mu_\kappa^0(\bullet) + \left[\dot{K}'(z,\bullet) + K^{0\prime}(z)\delta(\bullet)\right] * 2\eta(\bullet) + a_\kappa\left[\dot{K}(z,\bullet) + K^0(z)\delta(\bullet)\right] * 2\psi(\bullet)$$

$$+ \sum_j \left(\exp(\nu_j^0 t) - 1\right) \frac{\sin \beta_j a_\kappa z}{\beta_j a_\kappa} \kappa^2 (N_j - S_j) \qquad (46).$$

$$+ \sum_j C_j(z,t)\,\kappa^2 (N_j - S_j) + K^0(z)\,\kappa^2 (S_0 - S_\infty) - K(z,t)\,\kappa^2 S_0$$

Here K is the index blooming Green function Eq. (21), $K^0 \equiv K(t=0)$, superscript dot $\dot{}$ means d/dt, and

$$C_j(z,t) = \sum_{n=2}^{\infty} \sum_{m=1}^{n-1} \frac{\left(-\Gamma k z/\nu_j^0\right)^n \left(\nu_j^0 t\right)^m}{n!\,m!} \left[z\, j_n(a_\kappa z)\right] \qquad (47)$$

is the subexponential part of mode j. The relative minus sign between N_j and S_j is by convention; it is the same minus sign in Eqs. (23b) and (28). The transverse wavenumber κ is implied throughout; the field is an infinite superposition of modes at each transverse spatial frequency. Diffusion is neglected in Eq. (46); with diffusion all the Green functions and all the modes are multiplied by $\exp(-\mathcal{D}\kappa^2 t)$. The exponential part of mode j is a simple sinusoid in z with longitudinal wavenumber $\beta_j a_\kappa$. We will see in the next sections that at spatial frequencies with good phase correction ($g(\kappa) \approx 1$) the exponential part of mode 1, the fastest growing mode, dominates after a short time.

The modes and the free-running Green functions appear to violate energy conservation: in the linearized theory each transverse wavenumber is decoupled from all others, yet the energy in a wavenumber grows in time. But there is no paradox. Physically there are two energy sources in the linearized theory. First, in the STRS interaction the background plane wave scatters energy off μ into **F**. The growth of **F** is first order, but the balancing decrease of I_0 is second order so we do not see it. Second, the feedback control system can create and amplify perturbations by

transfering energy from the background plane wave to **F**. Again the growth of **F** is first order, but energy conservation is second order.

6. Fastest Growing Mode with Phase Correction

Phase-only correction with thermal blooming creates the exponentially growing unstable modes known as the phase compensation instability (PCI)[4-6]. There is a simple physical reason for PCI. Warm low-index spots in the fluid defocus the beacon. Phase reversal correction automatically focuses the intense beam into these spots heating them further. So phase correction makes hot spots hotter and cold spots colder.

Fig. 5 shows the dispersion relation of the mode 1 exponential growth rate ν_1 for perfect phase reversal correction in a uniform fluid. ν_1 is proportional to the "blooming rate" $\dot{N}_\lambda \equiv \Gamma kL/2\pi$ (waves/sec). Its asymptotic values are[4,6]

$$\begin{aligned} \nu_1 &\rightarrow \frac{4\pi\dot{N}_\lambda}{N_P} && \text{for } N_P >> 1 && \text{(geometric optics limit)} \\ &\rightarrow 4\dot{N}_\lambda && \text{for } N_P << 1 && \text{(diffractive limit)} \end{aligned} \qquad (48).$$

Small-scale or short wavelength perturbations with low Fresnel number are more unstable than large scales or long wavelengths, because short wavelength phase perturbations propagate more efficiently into log amplitude variations and consequently produce more heating over the path. Diffraction of very small scales causes phase and log amplitude to alternate along the path, so the instability growth rate in the diffractive limit asymptotes to a constant.

The end-of-path optical spectrum in the exponential part of mode 1 alone is

$$\Phi_1 \approx \langle\chi\chi^*\rangle_1 + \langle\phi\phi^*\rangle_1 = \exp(2\nu_1 t)\left[\left|\frac{\sin\beta_1\ell}{\beta_1}\right|^2 + |\cos\beta_1\ell|^2\right] k^2 \langle (N_1 - S_1)(N_1 - S_1)^* \rangle \quad (49),$$

where brackets <> mean an ensemble average over the noise as well as the random

index field. The residue factor $\nu_1^0 \partial\Delta/\partial\nu_1$ needed to calculate the source is shown in Fig. 6; it is $\mathcal{O}(1)$ over the region of practical interest. The mode propagation factor, $\left|\frac{\sin \beta_1 \ell}{\beta_1}\right|^2 + |\cos \beta_1 \ell|^2$, is shown in Fig. 7. The total energy in mode 1 summed over all spatial frequencies is

$$\mathcal{E}_1^* = 2\pi \frac{k}{L} \int_0^{\ell_{PC}} \Phi_1 \, d\ell \tag{50}$$

where ℓ_{PC} is the phase correction cutoff.

In the following sections we calculate the growth of Φ_1 from noise and turbulence. We are especially interested in the large scale or geometric optics limit, since the Fresnel cutoff of typical phase correctors for the atmosphere is large[10]. For simplicity we assume the beacon and intense wavelengths are equal(b = 1); also we drop the subscript 1 since all quantities are evaluated at $\nu = \nu_1$. Also we assume the noise and initial index are uncorrelated, $\langle NS^* \rangle = 0$.

7. Growth from Noise

We will calculate Φ_1 for two noise sources: (a) a pure log amplitude or phase fluctuation impulse for a short time Δt, and (b) a stationary Markov noise process. All noise sources N are calculated from Eq. (45).

The Laplace transform of an impulse perturbation f_o for a short time Δt is $\hat{f} = f_o \Delta t$. This is substituted into $\hat{\psi}$ or $\hat{\eta}$ in Eq. (45) to give the noise source

$$kN = \frac{1}{\nu \dfrac{\partial \Delta}{\partial \nu}} \left[\psi_o + \eta_o \frac{g \hat{B}_{\varphi i}}{a_\kappa} \right] \nu \Delta t \tag{51}.$$

At frequencies with perfect phase correction N simplifies further, since

$$\frac{g \hat{B}_{\varphi i}}{a_\kappa} = \frac{\beta \cos \ell}{\sin \beta \ell} \qquad \text{for } g = 1 \tag{52}.$$

At long wavelengths($\ell \to 0$) N simplifies even further, since

$$\lim_{\ell \to 0} \beta\ell = \pi/2$$

$$\lim_{\ell \to 0} \nu^{o} \frac{\partial \Delta}{\partial \nu} = \pi/4 \qquad (53).$$

Substituting Eqs. (48), (52), (53) into (51) and replacing ΔN_λ for $\dot{N}_\lambda \Delta t$, the noise source at large scales is

$$kN \underset{(\ell \to 0)}{\sim} \frac{64}{\pi^2} \Delta N_\lambda \left(\ell \psi_0 + \frac{\pi}{2} \eta_0 \right) \qquad (54).$$

In the geometric limit of correction, log amplitude noise is most effective at exciting exponential growth; in this limit the end-of-path perturbation is mainly log amplitude also.

We compared this theory to numerical simulations of propagation in blooming. The simulations were done with our computer code, ORACLE, which solves the full nonlinear wave-fluid problem on a discrete four-dimensional mesh. ORACLE represents the electric fields by two-dimensional complex number arrays and represents the fluid as a layered medium with a two-dimensional real density array for each layer. On each time step ORACLE propagates a beacon pulse backward and an intense pulse forward by split-operator FFT[13]; then the density arrays are convected for one time step and heated by one pulse. The intense beam can be phase compensated using information on the beacon phase.

The simulations were done for a square beam which fills the transverse mesh, and also for a round beam with apodized edge. The fluid had uniform Γ and v. A pure sinusoidal intensity perturbation (wavenumber κ) was introduced at z = 0 for one time step, then removed; all subsequent time evolution of this perturbation was due to the interaction between phase correction and blooming. Perfect phase reversal (g = 1) was done on every mesh point and time step. The growth rate was measured by $|E_\kappa|^2$, the electric field spectrum at path end. Whole beam Fresnel number N_F typically was

~10,000 , much larger than N_P. The computations were done on a Cray X-MP in 64-bit mode, with 128 and 256 transverse zones.

Typical results are shown in Figs. 8 and 9. Fig. 8 compares the analytical and computational growth rates. The measured dispersion relation is in excellent agreement with the leading singularity $\nu(\kappa)$. Fig. 9 compares the numerical time evolution from ORACLE to the growth of mode 1 from impulse noise, Eqs.(49) and (51). The agreement is excellent after a short time. [The spectrum eventually decays because the index perturbation is convected out of the laser beam.] The behavior at other Fresnel numbers is similar. Evidently, at wavenumbers with good compensation, mode 1 dominates for $N_\lambda \geq 0.1$ wave.

We consider two types of Markov noise process (b): (i) noise with a finite correlation time t_c, correlation function $\langle f(o)\, f^*(t)\rangle = \langle f\, f^*\rangle \exp(-|t|/t_c)$, and (ii) a discrete time series with time step Δt, correlation function $\langle f(o)\, f^*(t)\rangle = \langle f\, f^*\rangle \Theta(t)\ \mathrm{rect}(t/2\Delta t)$. The power spectrum of the Markov process is

$$\left\langle \hat{f}(\nu)\, \hat{f}^*(\nu)\right\rangle = \langle ff^*\rangle \begin{cases} \dfrac{1}{\nu\,(\nu + 1/t_c)} & \text{(i)} \\ \dfrac{1}{\nu^2}\,\dfrac{1 - \exp(-\nu\Delta t)}{1 + \exp(-\nu\Delta t)} & \text{(ii)} \end{cases} \qquad (55).$$

The two processes have the same form of power spectrum in the low frequency limit (νt_c and $\nu\Delta t << 1$) and the high frequency limit (νt_c and $\nu\Delta t >> 1$). We are mainly interested in modes with low frequencies (compared to the noise), i.e., $\nu_1 << 1/t_c$ or $<< 1/\Delta t$. Digital computer simulation of a noise process with no correlation between time steps makes a discrete time series. A digital simulation with time step $\Delta t << 1/\nu$ can be scaled to give the same mode 1 source as a Markov process with $t_c << 1/\nu$.

The random noise source for mode 1 at low frequencies, assuming uncorrelated log amplitude and phase, is

$$k^2\langle N\,N^*\rangle \;=\; \frac{1}{\left|\nu\dfrac{\partial\Delta}{\partial\nu}\right|^2}\left[\langle\psi\psi^*\rangle + \langle\eta\eta^*\rangle\left|\frac{g\hat{B}_{\varphi\,i}}{a_\kappa}\right|^2\right]\cdot\begin{cases} \nu t_c & \text{(i)} \\ \nu\Delta t/2 & \text{(ii)}\end{cases} \qquad (56).$$

In the geometric limit, and with the replacement of ΔN_λ for $\dot{N}_\lambda t_c$ or $\dot{N}_\lambda \Delta t/2$, this simplifies to

$$k^2\langle NN^*\rangle \underset{(\ell\to 0)}{\sim} \Delta N_\lambda \frac{256}{\pi^3}\left[\ell\langle\psi\psi^*\rangle + \frac{\pi^2}{4\ell}\langle\eta\eta^*\rangle\right] \qquad (57).$$

The asymptotic form of the propagation factor is

$$\left|\frac{\sin\beta\ell}{\beta}\right|^2 + \left|\cos\beta\ell\right|^2 \underset{(\ell\to 0)}{\sim} \frac{\ell^2}{(\pi/2)^2} \qquad (58).$$

Substituting these into Eq.(49), the low frequency and long wavelength spectrum from Markov noise is

$$\Phi_1 \underset{(\ell\to 0)}{\sim} \exp(2\nu t)\,\Delta N_\lambda \frac{256}{\pi^3}\left[\frac{4}{\pi^2}\ell^3\langle\psi\psi^*\rangle + \ell\langle\eta\eta^*\rangle\right] \qquad (59).$$

Notice that a spatially white noise process (f independent of κ) does not make a white noise optical spectrum. If the PC cutoff is at large scales, so $\nu \propto \ell$ over the entire spectrum, then by Eqs. (50) and (59) the total mode 1 energy excited by white noise is

$$\mathcal{E}_1^* \approx \Delta N_\lambda\left\{\frac{1024}{\pi^5}\ell_{PC}^3\,\Psi^2\left[\frac{\exp(G)(G^3 - 3G^2 + 6G - 6)}{G^4} + \frac{6}{G^4}\right] + \frac{256}{\pi^3}\ell_{PC}\,X^2\left[\frac{\exp(G)(G-1)}{G^2} + \frac{1}{G^2}\right]\right\} \qquad (60)$$

where $G = 8\pi N_\lambda/N_{PC}$ is the gain at the cutoff wavenumber (not the $\hat{G}$ control operator in Eq.(14)), and Ψ^2 and X^2 are the phase and log amplitude variances within the cutoff.

8. Growth from Turbulence

The mode 1 random index source from Eq.(44) is

$$k^2\langle SS^*\rangle = \int_0^L\int_0^L \left|\frac{g}{\nu^o\frac{\partial\Delta}{\partial\nu}}\right|^2 (1 - Q(s))(1 - Q^*(s'))\langle\mu^o(s)\,\mu^{o*}(s')\rangle\, ds\, ds' \qquad (61).$$

In the case of thermal turbulence this can be simplified by the standard Tatarskii analysis[11]:

$$k^2\langle SS^*\rangle \approx 2\pi k^2\Phi^o\int_0^L C_\mu^2(s)\left|\frac{g}{\nu^o\frac{\partial\Delta}{\partial\nu}}\right|^2 |1 - Q(s)|^2\, ds \qquad (62).$$

Eq.(62) is the rigorous formulation of a simple intuitive picture--the turbulent "seed" of instability is a propagation-weighted sum over the path. C_μ^2 measures the turbulence and $|1 - Q|^2$ measures propagation (Green function). The weighting tends to increase with distance out from the transmitter, as phase fluctuations propagate into amplitude fluctuations and heating inhomogeneities. Intuitively, with good phase correction the turbulence at the transmitter should not excite an instability; in fact for g=1 the weighting $1 - Q(0) = 0$.

If the turbulence is uniform or globally homogeneous then the range integral can be done,

$$\frac{2}{L}\int_0^L \left|\frac{g}{\nu^o\frac{\partial\Delta}{\partial\nu}}\right|^2 |1 - Q(s)|^2\, ds \equiv q(\kappa) =$$

$$\left|\frac{g}{\nu^o\frac{\partial\Delta}{\partial\nu}}\right|^2 \left\{\left[\cos^2\ell + \frac{\sin^2\ell}{|\beta|^2}\right]\frac{\sinh 2\mathrm{Im}(\beta\ell)}{2\mathrm{Im}(\beta\ell)} + \left[\cos^2\ell - \frac{\sin^2\ell}{|\beta|^2}\right]\frac{\sin 2\mathrm{Re}(\beta\ell)}{2\,\mathrm{Re}(\beta\ell)}\right. \qquad (63).$$

$$\left. + 2\sin\ell\cos\ell\left[\mathrm{Re}\left(\frac{1}{\beta}\right)\frac{\sin^2\mathrm{Re}(\beta\ell)}{\mathrm{Re}(\beta\ell)} - \mathrm{Im}\left(\frac{1}{\beta}\right)\frac{\sinh^2\mathrm{Im}(\beta\ell)}{\mathrm{Im}(\beta\ell)}\right]\right\}$$

Fig. 10 shows the q function over the range of interest. Substituting Eqs.(63) and (33) into (62) we obtain the mode 1 excitation by uniform turbulence:

$$k^2\langle SS^*\rangle = \frac{.245}{r_0^{5/3}} \frac{q(\kappa)}{\kappa^{11/3}} = .01215 \frac{L\, q}{k N_T^{5/6} \ell^{11/6}} \qquad (64).$$

The numerical factors are precisely

$$\frac{4}{3}\left(\frac{50}{3}\right)^{1/6} \frac{\Gamma^{5/6}(1/5)}{\Gamma^2(1/6)} \approx 0.245$$

and

$$\frac{1}{12}\left(\frac{50}{12}\right)^{1/6} \frac{\Gamma^{5/6}(1/5)}{\Gamma^2(1/6)} \approx 0.01215 \ .$$

The wave spectrum and Strehl ratio from turbulence are found by substitution of Eq. (64) into Eqs.(49) and (36).

Fig. 11 shows the mode 1 end-of-path spectrum growing from initially uniform turbulence. Notice the strong similarity between Φ_1 (Fig. 11) and the full Φ (Fig. 2) for wavenumbers $\kappa < \kappa_{PC}$. The initial spectrum at large scales is mainly log amplitude perturbation and decreases gradually as $\kappa^{1/3}$ or $N_P^{-1/6}$. Most of the initial uncorrected scintillation at large scales couples to mode 1: with perfect phase correction, at t = 0

$$\lim_{\ell \to 0} \frac{\Phi_1}{\Phi} = \frac{96}{\pi^4} \approx .985 \qquad (65).$$

Phase perturbation becomes more important at small scales. Φ_1 grows *exponentially* in time at rate $2\nu(\kappa)$ (Fig. 5). The long wavelength form is

$$\Phi_1 \underset{(\ell \to 0)}{\sim} (.0049) \frac{L}{k} \frac{\ell^{1/6}}{N_T^{5/6}} \exp(2\nu t) \qquad (66).$$

Curiously the initial spectrum (Fig. 11) is quasi-white noise over the wavenumber range of practical interest, $100 > N_P > 1$ or $0.15 < \kappa\sqrt{L/2k} < 1.5$. If the PC cutoff $N_{PC} > 1$ then the initial turbulence energy $\mathcal{E}_1$ in mode 1 is

$$\mathcal{E}_1 \approx \frac{(0.3 \text{ rad})^2}{N_T^{5/6} N_{PC}} \qquad (67).$$

Much of this wavenumber range has $\nu \propto \ell \propto \kappa^2$. For true white spatial noise with quadratic gain the amplified energy is

$$\mathcal{E}_1^* = \mathcal{E}_1 \frac{\exp(G) - 1}{G} \qquad (68)$$

where G is the gain at the highest wavenumber. If the PC cutoff is sufficiently large, say $N_{PC} \geq \pi$, then the mode 1 energy excited by turbulence will approximately follow Eq.(68) with $G = 8\pi N_\lambda / N_{PC}$:

$$\mathcal{E}_1^* \approx \frac{(0.3 \text{ rad})^2}{N_T^{5/6} N_{PC}} \frac{\exp(G) - 1}{G} = \frac{(.06 \text{ rad})^2}{N_T^{5/6}} \frac{\exp\left(\frac{8\pi}{N_{PC}} N_\lambda\right) - 1}{N_\lambda} \qquad (69).$$

Fig. 12 compares our two analytic predictions of perturbation growth from turbulence, the Taylor series $\Phi(t)$ (Eqs. (A9) - (A11)) and the leading exponential mode $\Phi_1(t)$ (Eqs.(49) and (64)). Agreement is excellent after a short time. At larger Fresnel numbers Φ becomes exponential even sooner. Evidently mode 1 dominates, at wavenumbers with good compensation, for $N_\lambda \geq 0.1$ wave.

9. Comparison to Numerical Results with Turbulence

Numerical simulations of thermal blooming in turbulence were done with the ORACLE code. The simulations used square mesh-filling beams and an atmosphere with uniform C_μ^2, Γ, v and $\mathcal{D}$. Each initial density screen had a Kolmogorov spectrum and Gaussian random phases in Fourier space. The control system response was modeled by a Fourier filter $g(\kappa)$ applied to the beacon phase before the phase reversal correction. The filter functions were supergaussian,

$$g(\kappa) = 2^{-\left(\kappa^2/\kappa_{pc}^2\right)^n} .$$

These filters have a smooth roll-off, but one may think of the nominal PC "cutoff" as the spatial frequency κ_{PC} where $g(\kappa_{PC}) = 1/2$. Fig. 13 shows the analytically-predicted mode 1 growth rate for various filter shapes. A significant range of wavenumbers was left uncorrected.

Fig. 14 compares the linearized theory spectrum (sum of χ and ϕ variances) to ORACLE simulations (numerical E-field variance) for three levels of turbulence. Numerical results are in excellent agreement with linearized theory, as long as the total energy $\mathcal{E}^*$ in all perturbations is small. This of course is the regime where we expect linearized theory to do well. The spectrum below cutoff exhibits the PCI exponential growth of mode 1. [The initial hesitation, and the shift of the PCI peak to a lower wavenumber, is because the fastest growing mode with filter $g(\kappa)$ is at a wavenumber slightly less than κ_{PC}; see Fig. 13. Systematic deviations from theory at the very lowest wavenumbers are due to non-Kolmogorov amplitudes in the initial density screens.] The spectrum above cutoff has the STRS growth of mode 0, with asymptotic STRS at very high wavenumbers[1,3]. For a mesh-filling beam the Strehl ratio is exactly $1 - \mathcal{E}^*$ by energy conservation. The Strehl ratio, Fig. 15, is dominated by exponential growth to saturation. Near saturation the spectrum is enhanced at harmonics of κ_{PC}, and also at all the corrected wavenumbers $\kappa < \kappa_{PC}$. At saturation the spectrum flattens and becomes unstructured, and the Strehl ratio rapidly falls to a low value. The behavior is similar for other values of the cutoff N_{PC}.

Numerical simulations of thermal blooming with good phase correction ($g(\kappa < \kappa_{PC}) \approx 1$ and initial Strehl ≈ 1) show essentially the same spectrum evolution for all levels of turbulence. With a fixed cutoff κ_{PC}, larger initial turbulence makes saturation occur sooner. But the phenomena of instability excitation and growth up to saturation are basically independent of initial turbulence. The same linear phenomena, scaled by $N_T^{-5/6}$, account for the spectrum and Strehl ratio at all levels of turbulence.

The departures of the numerical spectrum from theory near saturation arise from second and higher order nonlinear interactions ~ $\mathbf{F}^n$ dropped from the linearized theory. The mode-beating in these interactions generates perturbations at sum and difference wavenumbers, making energy cascade to ever-higher spatial frequencies. Frequency summing enhances the spectrum at harmonics of the largest perturbations, which typically are near κ_{PC}. Frequency differencing enhances the spectrum at low wavenumbers. Harmonics of κ_{PC} in the spectrum are common evidence of a closed-loop thermal blooming instability. The harmonics sometimes are masked by strong uncorrected turbulence at $\kappa > \kappa_{PC}$, but they reappear if open-loop growth is slightly damped by other phenomena.

At saturation and beyond, the optical and fluid fields break up into three–dimensional structures. The most common structures are filaments along the propagation direction. These look like "cells" in the transverse plane, as shown in Fig. 16. The cell size is equal to the PC cutoff wavelength $2\pi/\kappa_{PC}$, which means the structures are the result of PCI. Non-isotropic damping phenomena, which we will discuss later, change the 2D cells into stripes and the 3D filaments into ribbons.

Growth of perturbations by blooming has important consequences for the numerical simulation of propagation. The open and closed loop instabilities and the nonlinear cascade make perturbations grow at all wavenumbers out to the Nyquist frequency of the simulation. If the simulation is continued to sufficiently large blooming with little or no damping, then the results eventually are dominated by Nyquist noise and are no longer correct. Numerical results may even begin to violate physical constraints such as causality. The existence of small-scale thermal blooming instabilities explains the break-down of good numerical simulations. A large Nyquist energy, although usually symptomatic of a purely numerical code instability, is in this case physical and cannot be avoided in undamped thermal blooming.

10. Discussion

The last few sections analyzed in detail perturbation growth by thermal blooming in a fluid with uniform properties Γ, v, and C_μ^2. The results form a complete solution of linearized propagation in this simple and very idealized fluid. Growth from turbulence has simple asymptotic forms, Eq.(66) for phase corrected scales $\ell < \ell_{PC} << 1$ and Eq.(A9) for uncorrected scales $\ell \geq 1$. Intermediate scales $\ell \sim 1$ have more complex behavior given by the exact forms, Eqs.(A9) - (A11) and (49),(63),(65).

The main interest in perturbation growth is how it affects beam focusability. Perturbations significantly degrade beam focusability and far-field quality when their total energy summed over all scales approaches 1 radian, or $\mathcal{E}^* \sim 1$. [An exceptional case is when the perturbations are highly structured or have precisely the right phase between different scales to act as a "phased array" of sources with good far-field beam quality. This is not expected to occur either spontaneously from random turbulence excitation or dynamically from nonlinear phase locking.]

Perturbations will grow by thermal blooming if and only if the instability growth rates exceed the damping rates from other phenomena. Then net growth occurs, until stopped by (a) convection clearing, or (b) the nonlinear blooming interaction itself, i.e. the slowdown and saturation of growth when perturbations are large. Of course at saturation the beam already is degraded.

N_{crit} is the amount of blooming, measured in waves, needed to saturate the perturbations. If the small-scale instabilities are present and growing, then N_{crit} is the threshold for significant beam degradation and the maximum amount of blooming that can theoretically be compensated. In a laser beam of average power P and diameter D, $N_\lambda \propto P/D$, so N_{crit} also sets a maximum correctable power. This constraint often is more severe than the well-known whole-beam blooming constraint,[7,9] which sets a maximum value of $N_\lambda/N_F \propto P/D^3$.

Of practical interest is the limitation imposed by perturbation growth on laser propagation in the atmosphere. In the linearized theory the only damping phenomenon in a uniform atmosphere is diffusion. Atmospheric diffusivity $\mathcal{D} \sim 0.2\ cm^2/sec$ provides strong damping near the Kolmogorov inner scale(typically a few millimeters) but is too weak to damp scales around r_o (typically 10cm in visible light). In our simple uniform atmosphere, perturbations will grow according to linearized theory until $\mathcal{E}^* \sim 1$, and then growth will saturate after the beam is degraded.

It is straightforward to estimate the threshold waves of blooming N_{crit} needed to saturate the perturbations induced by turbulence. One can get a rough estimate and a scaling law from the asymptotic spectra, or a more accurate estimate by integration of the exact spectrum, Eqs. (A9) - (A11). One finds that for appropriate ranges of atmospheric turbulence ($r_o \sim 5$ - 50cm), path length (L ~ 1 - 3km) and phase control cutoff ($N_{PC} \geq N_T$) the intense beam will be much degraded after only a few waves of blooming.

However, this estimate has little or no practical significance, because the real atmosphere and adaptive optics differ from the simple analytical model in some important respects. In order to predict the saturation point in the real atmosphere we must consider the effect of: nonuniform distribution of properties, the limited spatiotemporal response of phase corrective adaptive optics, wind shear along the path, and velocity turbulence. We discuss each of these in turn.

The variation of Γ, $\mathcal{D}$ and C_n^2 along an atmospheric path is a technical feature that changes some quantitative details but does not change the general picture of rapid growth to saturation. The change of parameters is most significant along vertical paths. Most of the absorption and turbulence is in the planetary boundary layer extending less than 2km above ground level. Along vertical paths the appropriate length unit is not total path length L but an absorption scale length L_a defined, for example, as the range where $\alpha(L_a)\ \mathcal{T}(L_a) = e^{-1}\alpha(0)$; the appropriate dimensionless length is $\ell \equiv a_\kappa L_a$, and the

appropriate blooming rate is $\dot{N}_\lambda \equiv \Gamma(0)kL_a/2\pi$. An infinite atmosphere in which α and Γ decrease exponentially with z is somewhat more unstable than a simple uniform atmosphere of depth L_a because of thermal blooming at long range with small Fresnel number, although an exponential profile only L_a deep (1 e-fold) is somewhat less unstable than the uniform case because it has blooming concentrated at short range with larger Fresnel number; see Fig. 17. Nonuniform C_n^2 affects the source term Eq. (62), but this has only a logarithmic effect on the saturation threshold N_{crit}.

Real adaptive optics for phase correction would not work quite like the Fourier gain $g(\kappa, \nu)$ in linearized theory. Adaptive optics would have a discrete lattice pattern of sensors and actuators[10] with a space-variant response. Unstable correction modes on a lattice with spacing d are superpositions of κ-modes that differ by an integer multiple of the spatial sampling wavenumber $\kappa_d = \pi/d$, analogous to Bloch modes in a solid. The mathematical expression of PC control is Eq. (14) with the **G** operator mixing the κ-modes but diagonal in the lattice modes. Closed-loop instability growth occurs whenever the feedback system can create filament and ribbon structures in the refractive index. With real adaptive optics the feedback would be fixed to the lattice, while the structures would be fixed in the convected air. In the absence of wind, a null-seeking PC control system on the discrete lattice would have instabilities which are similar to the pure Fourier mode theory discussed earlier; the mode 1 growth rate (fastest growing mode) of the null-seeker is the same as Fig. 5 and Eq. (48), since the control system could create phase perturbations that are indistinguishable on the lattice from pure Fourier modes with $\kappa < \kappa_d$. Any wind, even uniform wind, would act to decouple the feedback (on the discrete lattice) from the refractive index (in the air), reducing the instability near κ_d. Consequently, instability growth of a discrete PC control system would differ significantly from the pure Fourier mode theory whenever the nascent filament and ribbon structures are convected across the lattice at a rate comparable to their growth rate, or $\kappa_d \cdot \mathbf{v} \sim \nu$. Also, in the very process of correction

real adaptive optics probably would create perturbations at wavenumbers above its own sampling frequency (fitting error), which would be a source for mode 0 open loop growth. These features can be modeled in linearized theory[18] to estimate their effect on saturation threshold.

Nonuniform wind velocity, or "wind shear", can significantly damp perturbations. Optical perturbations grow by creating refractive index perturbations that are correlated with and reinforce the optical perturbations. In the average convected frame of the fluid the perturbations are filaments of alternating high and low irradiance, and low and high index. Motion of one part of the atmosphere relative to another scrambles and breaks up these filamentary perturbations. The scrambling is a damping process competing with instability growth. Scrambling occurs only for wavevectors $\kappa \parallel \frac{\partial \mathbf{v}}{\partial z}$; there is no scrambling for wavevectors $\kappa \perp \frac{\partial \mathbf{v}}{\partial z}$.

The effect of wind shear depends on whether or not the damping rate exceeds the growth rate. We quantify this by a dimensionless shear equal to the ratio of the "rate of scrambling" to the "rate of blooming". There is some arbitrariness in the definition of each rate. We define "rate of blooming" as $\dot{N}_\lambda$, and we define "rate of scrambling" as the velocity variation divided by a scale length.

The velocity variation is quantified by the eigenvalues of the shear tensor. The shear tensor is defined as

$$\mathbf{C} \equiv \frac{1}{L_a} \int_0^{L_a} (\mathbf{v}(z) - \mathbf{v}_{ave})(\mathbf{v}(z) - \mathbf{v}_{ave})\, dz \qquad (70)$$

where $\mathbf{v}_{ave} \equiv \frac{1}{L_a} \int_0^{L_a} \mathbf{v}(z)\, dz$,

and the velocity variation is defined as

$$\Delta v_\pm \equiv \sqrt{12}\,[\text{eigenvalues}]^{1/2} = \sqrt{6}\left[\text{Tr}\,\mathbf{C} \pm \sqrt{(\text{Tr}\,\mathbf{C})^2 - 4\det \mathbf{C}}\right]^{1/2} \qquad (71).$$

If the wind shear is linear $\left(\frac{\partial \mathbf{v}}{\partial z} \text{ a constant independent of } z\right)$ then

$$\Delta v_+ = |\mathbf{v}(L_a) - \mathbf{v}(0)|, \qquad \Delta v_- = 0 \qquad \text{(linear shear)} \tag{72a}$$

If the wind field $\mathbf{v}(z)$ is a random function of distance along the propagation direction, with 1-axis standard deviation σ_v, then

$$\Delta v_\pm = \sqrt{12}\ \sigma_v \qquad \text{(random wind)} \tag{72b}$$

The dominant phenomena fix the scale length. A Fresnel zone width $\sqrt{\lambda L}$ is the appropriate scale length for scintillations, often the most important perturbation in the atmosphere. A diffusion scale length proportional to $\sqrt{\mathscr{D}}$ often is appropriate in laboratory experiments or other situations of strong thermal diffusion.

Referenced to a Fresnel zone the dimensionless shear[4] S is defined as

$$S_\pm \equiv \frac{\Delta v_\pm / \sqrt{4\lambda L_a/\pi}}{\dot{N}_\lambda} \tag{73}$$

This is a rigorous scaling parameter like N_λ and N_P, in the sense that the Green functions depend on wind shear through $S_\pm$ and not on $\Delta v_\pm$. For example, in a linear wind shear pattern the β function of Eq. (9) is

$$\beta^2 = 1 + \frac{16\, N_P/\pi}{\frac{\nu^o}{\dot{N}_\lambda} - 2\pi i \frac{S_+}{\sqrt{N_P}} \cos(\kappa, \mathbf{v}) \frac{z}{L_a}} \quad .$$

Since the Green functions depend on $\mathbf{v}(z)$ through β, Eq. (9), all linear shear profiles with the same S_+ have the same instability behavior.

The damping effect of linear wind shear is shown in Fig. 18. The mode 1 PC instability is completely suppressed for all perturbations $\kappa \| \frac{\partial \mathbf{v}}{\partial z}$ if $S_+ > 5$. Damping of the the mode 0 open loop STRS instability is easier, with essentially complete suppression if $S_+ > 1$. Perturbations $\kappa \perp \frac{\partial \mathbf{v}}{\partial z}$ are unaffected by linear wind shear. Growth of these perturbations in linear shear produces three-dimensional ribbon structures that give the beam a "striped" appearance in the transverse plane, as shown in Fig. 19. The

ribbons align parallel to $\frac{\partial \mathbf{v}}{\partial z}$. The unstable region of the two dimensional transverse κ-space contracts as the value of linear wind shear S_+ increases, eventually shrinking down to a narrow band along $\kappa || \frac{\partial \mathbf{v}}{\partial z}$. The saturation threshold N_{crit} only increases logarithmically with S_+ as the unstable region of phase space shrinks.

11. Turbulent Flow

Random isotropic wind shear should damp perturbations in all directions. Turbulent flow generates a random wind field which may provide such damping. Turbulent flow is common in the atmosphere; one finds it for example in the planetary boundary layer, which varies in thickness from a few hundred meters to several kilometers, and in the boundary layer around a moving vehicle.

Kinetic turbulence produces a random wind field which typically is locally isotropic and homogeneous with Kolmogorov spectrum in the inertial subrange[14]. This random field can be thought of as arising from the rotation of eddies of all sizes between the inner and outer scale. The small eddies produce a small random variation of velocity in all coordinates and in particular make the velocity at each range z a random function of the transverse coordinates and the time. This goes beyond the standard blooming model[7], Eqs. (1) and (2), which has $\mathbf{v}(z)$ dependent only on range z; we discuss this later. The large eddies produce a random z-variation of the transverse fluid velocity, which is unchanged on a time scale much longer than the time needed for instability growth or wind clearing. The large eddy turbulence is consistent with the standard model as random wind shear.

Large eddy turbulence can be modeled as a velocity realization of a Gaussian random function of z with appropriate power spectrum. Every realization is physically correct at t = 0. A time-independent realization remains correct over time intervals shorter than the time scale of changes in the large eddy rotation (typically several

seconds or more). For longer times the realization fails to follow the true velocity dynamics, but the statistical properties of the model are correct at long time if $< \mathbf{v}\mu >$ correlations are stationary.

A discrete element version of this model is used in the ORACLE code for propagation simulations[15, 16]. ORACLE generates random x and y wind fields as independent Markov processes in z. The Markov spectrum is determined by a correlation length L_c and a rms fluctuation σ_v. The Markov spectrum is a good model of the long wavelength turbulence at scales as large or larger than the outer scale, and it matches smoothly to the Kolmogorov spectrum at short wavelengths. The dimensionless shear of the random wind is

$$S = \frac{\sqrt{3\pi}\,\sigma_v}{\dot{N}_\lambda \sqrt{\lambda L_a}} \qquad (74).$$

A nonrandom velocity field is added to represent the average wind profile.

Random isotropic wind shear from large eddy rotation damps perturbations in all directions. Some ORACLE simulations are shown in Fig. 20. The open-loop STRS instability is suppressed by a low value of random shear, S ~ 1-2. At low values of shear the perturbations still grow by exponential PCI, as shown by the example in Fig. 21, and the usual filament and ribbon structures occur. All the instabilities, PCI as well as STRS, are suppressed by random shear greater than a threshold value S_{crit}. With $S > S_{crit}$ the spectrum grows no faster than linearly as the index perturbations generated by the intense laser are rapidly scrambled, the Strehl ratio declines slowly without any rapid fall, and the filament and ribbon structures do not occur. S_{crit} depends on N_{PC}: a shorter cutoff wavelength means faster PCI growth, which requires faster scrambling (larger S) for suppression.

The stability threshold in wind shear shear is equivalent to two other thresholds, which may have more direct physical appeal. Random wind suppresses all instabilities if the blooming *rate* is below threshold,

$$\dot{N}_\lambda < \dot{N}_{crit} \equiv \frac{\sqrt{3\pi}\,\sigma_v}{S_{crit}\sqrt{\lambda L_a}} \qquad (75).$$

or equivalently if the *absorbed irradiance* is below threshold,

$$\alpha L_a I_o < A_{crit} \equiv \frac{\sqrt{3\pi}}{\mathcal{M}} \sqrt{\frac{\lambda}{L_a}}\, \frac{\sigma_v}{S_{crit}} \qquad (76).$$

If a strong damping phenomenon like random wind shear is present, then $\dot{N}_{crit}$ is the maximum rate of blooming that can be stably compensated. $\dot{N}_\lambda \propto P/D^2$, so $\dot{N}_{crit}$ also sets a maximum correctable power. The constraint of $\dot{N}_\lambda < \dot{N}_{crit}$ usually is more modest than $N_\lambda < N_{crit}$. Consequently, isotropic damping of perturbations by random wind shear is the preferable condition for atmospheric propagation. Isotropic damping is provided by naturally occurring large eddy turbulence. Isotropic damping also could occur in a nonrandom wind field with sufficient shear in both directions. We studied the random shear threshold with ORACLE simulations. The simulations used round apodized beams in a model atmosphere with exponential absorption profile. We identified the threshold (rather imprecisely) by the absence of a rapid Strehl drop before the wind clearing time. The threshold did not seem to depend on the outer scale length L_c, for $L_c <$ a few hundred meters. We found the shear threshold for $10 < N_{PC} < 40$ to be approximately

$$S_{crit} \approx \frac{54 \pm 2}{N_{PC}} \qquad (77),$$

$$\text{or} \qquad \dot{N}_{crit} \approx \frac{(.057)\, N_{PC}\, \sigma_v}{\sqrt{\lambda L_a}} \qquad (78).$$

This means, for example, the threshold absorbed irradiance for instability growth of a 1 μm wavelength laser in air (thermal response $\mathcal{M} = 8.25 \times 10^{-4}$ cm^3/J) with a 2 km absorption depth would be approximately

$$\alpha L_a I_o \, (W/cm^2) \approx (0.15) \, N_{PC} \, \sigma_v \, (m/s) \qquad (79).$$

These numerically derived S_{crit} thresholds seem to be proportional to N_{PC}^{-1}. General theoretical arguments[4], valid for infinite beams and very short correlation length L_c, predict that the S_{crit} should be proportional to $N_{PC}^{-1/2}$. The discrepancy may be due to the finite beam, the correlation length, or the numerical uncertainty in identifying S_{crit}. Much more study is needed to determine the sensitivity of the threshold to all the propagation parameters.

Small-eddy rotation could produce significant damping if it has a local shear >> 1. However, the smaller eddies move slower than the large eddies (their faster rotation rate is more than offset by their smaller size), so scrambling by turbulent flow gets less effective as scale size decreases. The speed of eddies ~r_o in size in the air is usually much less than large eddy random wind shear, and usually the local shear is < 1, so we expect that small-eddy or local turbulence in the air typically has only a small effect on perturbation growth.

Small-eddy rotation also produces turbulent mixing i.e. the local transport of thermal inhomogeneities inside the beam path. Turbulent mixing breaks up large-scale thermal structures. Averaged over long time this looks like diffusion, and is sometimes called "eddy diffusivity". But turbulent mixing is not diffusive over short times (such as an instability growth time). True diffusion would erase the Kolmogorov spectrum of thermal fluctuations. Turbulent mixing *maintains* the Kolmogorov spectrum in the inertial subrange. It does this by transferring energy to ever-higher wavenumbers and smaller scales; this is sometimes called a Richarson cascade. The cascade finally ends at the Kolmogorov inner scale, where viscosity and thermal diffusion dominate over mixing. Consequently, small-eddy turbulence may *excite* the instability at higher wavenumbers while it damps the instability at lower wavenumbers.

We limited most of our discussion to phase-only correction, but there are other methods of optical control that should be considered. Methods that control the intensity as well as the phase of the intense laser beam have lower instability growth rates than PC, and full electric field conjugation is stable at all controlled spatial frequencies[4]. These other control laws have different spectral evolution from PC, and they have different thresholds. Because it has smaller closed-loop growth rates, full field conjugation, and intensity and phase control that mimics full conjugation, has a significantly higher threshold absorbed irradiance for instability growth and a lower critical shear for instability suppression.

12. Conclusion

We have extended the linearized propagation theory to include the combined effects of turbulence, thermal blooming and dynamic phase correction. The exact open and closed-loop Green functions of the simple uniform fluid provide powerful tools to study these interactions. Some of the complex behavior seen in digital propagation simulations now can be broken down into simple well-understood growth and damping phenomena, at least while the perturbations are small. One can predict instability growth rates and predict excitation strengths from homogeneous turbulence. Of practical importance, one can understand the thresholds at which damping phenomena suppress instability growth, and understand the threshold scaling. Random wind shear from large-eddy rotation seems to be the most powerful damping effect in the atmosphere. When the instabilities are suppressed, the perturbations on corrected beams start small and stay small. This of course is precisely the regime where we expect the linearized theory to work.

If the damping phenomena are too weak then perturbations grow rapidly, especially at high wavenumbers, until they saturate at large amplitude and degrade the beam quality. Digital simulations at saturation show nonlinear energy cascading,

transverse pattern formation, and some evidence of chaos, e.g. strange attractors. The linearized theory and Green functions alone obviously cannot explain the saturation dynamics. This regime is of intrinsic interest in the theory of nonlinear wave propagation, but some further theoretical development is required to fully understand it. Fortunately this regime is relevant to practical applications mainly by avoidance.

We believe that our methods and some of our results will be useful for other problems of wave propagation. For example, the closed-form Green functions for phase correction (without blooming) may be applied to the theory of imaging and propagation through turbulence.

Acknowledgement

We have benefited from stimulating conversations with Alex Glass, Keith Brueckner, Marshall Rosenbluth, William Dannevik and James I. Davis. This research was performed under the auspics of the U.S. Department of Energy by Lawrence Livermore National Laboratory under contract W-7405-Eng-48, for the U. S. Army in support of funding order No. W31RPD-7-D4041.

Appendix

The general form of the field spectrum can be calculated for the case of uniform initial turbulence. The spectrum consists of three separate parts: the open loop Φ_{OL}, closed loop Φ_{CL}, and mixed Φ_M terms. These are obtained from substituting the expressions for $\langle \chi\chi^* \rangle$ and $\langle \phi\phi^* \rangle$ found in the text (Eq. (31)) into the definition for the spectrum, $\Phi = \langle \chi\chi^* \rangle + \langle \phi\phi^* \rangle$. At the path end (z = L):

$$\Phi_{OL} = \frac{.0243}{kN_T^{5/6}\,\ell^{11/6}} \int_0^L \left[K'^2(L - s, t) + a_\kappa^2 K^2(L - s, t)\right] ds \qquad \text{(A1)}$$

$$\Phi_M = -\frac{.0243}{kN_T^{5/6}\,\ell^{11/6}} 2 \int_0^L \left[K'(L - s, t)\, K^{PC'}(L|\, s, t) + a_\kappa^2 K(L - s, t)\, K^{PC}(L|\, s, t)\right] ds \qquad \text{(A2)}$$

$$\Phi_{CL} = \frac{.0243}{kN_T^{5/6}\,\ell^{11/6}} \int_0^L \left[K^{PC'^2}(L|\, s, t) + a_\kappa^2 K^{PC^2}(L|\, s, t)\right] ds \qquad \text{(A3)}.$$

Taylor series expansions for each term are obtained from the generalized two-time spectrum $\Phi(t, t') = \langle \chi(t)\, \chi^*(t') \rangle + \langle \phi(t)\, \phi^*(t') \rangle$. This reduces to the ordinary single-time spectrum when t′= t. The generalized spectrum consists of three parts corresponding to the open loop, closed loop, and mixed terms given above. The series expansions for Eqs. (A1), (A2), and (A3) are obtained by first inverting the double Laplace transforms of the corresponding terms in the two-time spectrum, then setting t′= t. The double Laplace transforms of the terms corresponding to Eqs. (A1), (A2), and (A3) are

$$\hat{\Phi}_{OL} = \frac{.0243}{kN_T^{5/6}\,\ell^{11/6}} \int_0^L \left[\hat{K}'(L - s, \nu)\, \hat{K}'(L - s, \nu') + a_\kappa^2 \hat{K}(L - s, \nu)\, \hat{K}(L - s, \nu')\right] ds \qquad \text{(A4)}$$

$$\hat{\Phi}_M = -\frac{.0243}{kN_T^{5/6}\,\ell^{11/6}}\int_0^L \left[\hat{K}'(L-s,\nu)\,\hat{K}^{PC'}(L|s,\nu') + \hat{K}'(L-s,\nu')\,\hat{K}^{PC'}(L|s,\nu)\right. \tag{A5}$$

$$\left. + a_\kappa^2\,\hat{K}(L-s,\nu)\,\hat{K}^{PC}(L|s,\nu') + a_\kappa^2\,\hat{K}(L-s,\nu')\,\hat{K}^{PC}(L|s,\nu)\right] ds$$

$$\hat{\Phi}_{CL} = \frac{.0243}{kN_T^{5/6}\,\ell^{11/6}}\int_0^L \left[\hat{K}^{PC'}(L|s\,\nu)\,\hat{K}^{PC'}(L|s,\nu') + a_\kappa^2\,\hat{K}^{PC}(L|s,\nu)\,\hat{K}^{PC}(L|s,\nu')\right] ds \tag{A6}.$$

After the substitutions $\hat{K}^{PC}(z|s) = \hat{K}(z)\,\hat{M}(s)$, $\hat{K}(z) = \sin(a_\kappa\beta z)/\nu a_\kappa\beta$, each of these expressions becomes a sum of terms of the form

$$\frac{1}{\nu-\nu'}\left[F(\nu)\,G(\nu') - G(\nu)\,F(\nu')\right] \tag{A7}.$$

The double inverse transform of (A7) is given by

$$\int_0^t \left[f(t-\tau)\,g(t'+\tau) - g(t-\tau)\,f(t'+\tau)\right] dt \tag{A8}$$

where f and g are the inverse Laplace transforms of F and G respectively. Repeated application of this result gives the general inverse transform for each part of the generalized spectrum. Taylor expansions of each term allow the time integral to be evaluated. The final expressions for the parts of the single-time spectrum are obtained by setting $t' = t$:

$$\Phi_{OL}(\ell, \theta) = \frac{.0243L}{k\, N_T^{5/6}\, \ell^{11/6}} \left\{ 1 - \frac{\theta}{\ell}\left[1 - \frac{\sin(2\ell)}{2\ell} \right] + \right.$$

$$+ \sum_{n=2}^{\infty} \frac{(-\theta)^n}{n!\,(n+1)!} \left[2^n \left(\ell\, j_n(\ell) \sin \ell - h_n(\ell) \cos \ell \right) \right]$$

$$\left. + (n+1)\,\ell \sum_{m=0}^{M_n} \binom{n}{m} \binom{n}{m+1} a_m (n-1) \left(h_m(\ell)\, j_{n-m-1}(\ell) - j_m(\ell)\, h_{n-m-1}(\ell) \right) \right\} \qquad \text{(A9)}$$

$$\Phi_M(\ell, \theta) = -\frac{.0243\ L}{k\, N_T^{5/6}\, \ell^{11/6}}\, g \left\{ \sum_{p=2}^{\infty} (-2\theta)^p \sum_{q=0}^{Q_p} \frac{a_q\,(p-1)}{q!\,(p-q-1)!} \right.$$

$$\cdot \left[\frac{1}{2^{q+1}\,(q+1)!} \sum_{m=0}^{p-q} \frac{(-1)^m\, T_m(\ell)}{m!\,\ell^m} \frac{D_{q+1,\,p-q-m}(\ell)}{(p-q-m)!} \right.$$

$$\left. \left. - \frac{1}{2^{p-q}\,(p-q)!} \sum_{m=0}^{q+1} \frac{(-1)^m\, T_m(\ell)}{m!\,\ell^m} \frac{D_{p-q,\,q+1-m}(\ell)}{(q+1-m)!} \right] \right.$$

$$\left. + \sum_{p=0}^{\infty} \frac{(-4\theta)^p}{p!} \left[\sum_{m=0}^{p} \frac{(-1)^m\, T_m(\ell)}{m!\,\ell^m} \frac{D_{o,\,p+1-m}(\ell)}{(p+1-m)!} - \frac{D_{p+1,\,o}(\ell)}{2^{p+1}\,(p+1)!} \right] \right\} \qquad \text{(A10)}$$

$$\Phi_{CL}(\ell, \theta) = \frac{.0243\ L}{k\, N_T^{5/6}\, \ell^{11/6}}\, g^2 \left[\sum_{p=2}^{\infty} \left(\frac{2\theta}{\ell}\right)^p \sum_{q=0}^{Q_p} \frac{a_q\,(p-1)}{q!\,(p-q-1)!} \right.$$

$$\bullet \sum_{n=0}^{q+1} \sum_{m=0}^{p-q} \frac{T_m(\ell)\, T_n(\ell)}{m!\, n!}\, A_{q-n+1,\,p-q-m}(\ell)$$

$$+ \sum_{p=0}^{\infty} \frac{1}{p!} \left(\frac{4\theta}{\ell}\right)^p \sum_{m=0}^{p} \frac{T_m(\ell)}{m!}\, A_{o,\,p-m+1}(\ell) \qquad \text{(A11)}$$

$$\left. + \ell \sin\ell \cos\ell \sum_{p=0}^{\infty} \left(\frac{2\theta}{\ell}\right)^p \sum_{q=0}^{p} \frac{1}{q!\,(p-q)!} \sum_{n=0}^{q} \sum_{m=0}^{p-q} \frac{(-\ell)^{m+n}\, T_{q-n}(\ell)\, T_{p-q-m}(\ell)}{(q-n)!\,(p-q-m)!}\, B_{m\,n}(\ell) \right]$$

where

$$A_{mn}(\ell) = \frac{\ell\,(-\ell)^{m+n}}{m!\,n!} \left\{ (1 + \cos^2\ell)\left[j_{m-1}(2\ell)\, j_n(2\ell) - j_m(2\ell)\, j_{n-1}(2\ell) \right] \right.$$

$$\left. + \frac{m-n}{\ell} \cos^2\ell\, j_{m-1}(2\ell)\, j_{n-1}(2\ell) \right\}$$

$$+ \ell^2 (-\ell)^{m+n} \sin^2\ell \left[\frac{j_m(2\ell)}{2^n\, m!} \sum_{q=0}^{n} \frac{j_q(\ell)\, j_{n-q}(\ell)}{q!\,(n-q)!} \right. \qquad \text{(A12a)}$$

$$\left. - \frac{j_n(2\ell)}{2^m\, n!} \sum_{q=0}^{m} \frac{j_q(\ell)\, j_{m-q}(\ell)}{q!\,(m-q)!} \right] \quad , \quad m \geq 1$$

$$A_{on}(\ell) = \frac{(-\ell)^n}{n!} \cos(2\ell)\, j_n(2\ell) - \left[\frac{n}{\ell}\cos^4\ell + \sin\ell\cos\ell\,(1 + \cos^2\ell)\right] j_{n-1}(2\ell)$$

$$+ \frac{\ell}{2^n}\sin^3\ell\cos\ell \sum_{q=0}^{n}\binom{n}{q} j_q(\ell)\, j_{n-q}(\ell)\Bigg\}, \quad n\geq 1 \qquad \text{(A12b)}$$

$$A_{oo}(\ell) = 0 \ , \qquad \text{(A12c)}$$

$$B_{mn}(\ell) = \frac{j_m(2\ell)\, j_n(2\ell)}{m!\, n!} + \frac{\ell^2}{2^{m+n}} \sum_{p=0}^{m}\sum_{q=0}^{n} \frac{j_p(\ell)\, j_{m-p}(\ell)\, j_q(\ell)\, j_{n-q}(\ell)}{p!\, q!\, (m-p)!\, (n-q)!} \ , \qquad \text{(A13)}$$

$$D_{m\,n}(\ell) = \ell\sin\ell \quad 2\ell\, j_m(\ell)\, j_n(2\ell) - 2m\, j_{m-1}(\ell)\, j_n(2\ell) + \ell\, j_{m-1}(\ell)\, j_{n-1}(2\ell)$$

$$- \frac{\ell^2}{2^n} j_{m-1}(\ell) \sum_{p=0}^{n}\binom{n}{p} j_p(\ell)\, j_{n-p}(\ell)\Bigg]$$

$$- \ell\cos\ell\,[2\ell\, j_{m-1}(\ell)\, j_n(2\ell) \qquad \text{(A14a)}$$

$$- (2m-n)\, j_{m-1}(\ell)\, j_{n-1}(2\ell) - 2\ell\, j_m(\ell)\, j_{n-1}(2\ell)] \ , \ m, n \geq 1$$

$$D_{on}(\ell) = \frac{3\ell}{2}\sin(2\ell)\, j_{n-1}(2\ell) - 2\ell\cos(2\ell)\, j_n(2\ell)$$

$$+ \frac{\ell}{2^n}[\cos\ell\, j_n(\ell) - \sin\ell\, j_{n-1}(\ell)] + n\cos^2\ell\, j_{n-1}(2\ell)$$

$$- \frac{\ell^2\sin(2\ell)}{2^{n+1}} \sum_{q=0}^{n}\binom{n}{q} j_q(\ell)\, j_{n-q}(\ell) \ , \ n \geq 1 \qquad \text{(A14b)}$$

$$D_{mo}(\ell) = \ell \cos \ell\, j_m(\ell) - \ell \sin \ell\, j_{m-1}(\ell) - 2m \cos \ell\, j_{m-1}(\ell) \quad , \quad m \geq 1 \tag{A14c}$$

$$D_{oo}(\ell) = 0 \tag{A14d}$$

$$T_n(\ell) = -g\ell \sum_{m=0}^{n-1} \left(-\frac{\ell}{2}\right)^{n-m} \binom{n}{m} T_m(\ell)\left[\sin \ell\, j_{n-m}(\ell) + \cos \ell\, j_{n-m-1}(\ell)\right] , \tag{A15a}$$

$$T_o(\ell) = 1 \tag{A15b}$$

$$h_n(\ell) = n\, j_n(\ell) - \ell\, j_{n-1}(\ell) , \tag{A16}$$

$$a_m(n) = \int_0^1 \left[(1-t)^m (1+t)^{n-m} - (1-t)^{n-m}(1+t)^n\right] dt , \tag{A17}$$

M_n is the integer part of n/2 - 1, Q_p is the integer part of p/2 - 1, and $j_n(\ell)$ are the spherical Bessel functions of order n. The numerical factor in Eqs. (A9) - (A11) is precisely

$$\frac{1}{6}\left(\frac{25}{6}\right)^{1/6} \frac{\Gamma^{5/6}(1/5)}{\Gamma^2(1/6)} \approx 0.0243 .$$

References

1. K. A. Brueckner and S. Jorna, "Linearized theory of laser-induced instabilities in liquids and gases", Phys. Rev. 164,182-193 (1967); N. M. Kroll and P. L. Kelley, "Temporal and spatial gain in stimulated light scattering", Phys. Rev. A4, 763-776 (1971).

2. K. S. Gochelashvili, I. V. Chasei, and V. I. Shishov, "Instability of a light pulse in a nonlinear delayed-response scattering medium,", Sov. J. Quan. Elec. 10,1207-1209 (1980); V. S. Averbakh, A. A. Betin, V. A. Gaponov, A. I. Makarov, G. A. Pasmanik, and V. I. Talanov, "Induced scattering and self-action in gases and their effect on propagation of optical radiation (survey)", Izv. Vyssh. Uch. Zav. Radiof. 21, 1077-1106 (1978).

3. D. H. Chambers, T. J. Karr, J. R. Morris, J. A. Viecelli, P. Cramer and A. K. Gautesen, "Linear theory of uncompensated thermal blooming in turbulence," Lawrence Livermore National Laboratory report UCID-21696, 7 February 1989. (to be pubhlised in Phys. Rev. A)

4. T. J. Karr, "Thermal blooming compensation instabilities", Lawrence Livermore National Laboratory report UCID-21172, 14 August 1987; J. Opt. Soc. Am. A6, 1038(1989)

5. J. R. Morris, "Standard Green's function derivation of the thermal blooming compensation instability equations", Lawrence Livermore National Laboratory report UCID-21261, 14 October 1987 (to be published in J. Opt. Soc. Am. A, Dec. 1989).

6. R. J. Briggs, "Models of high spatial frequency thermal blooming instabilities", Lawrence Livermore National Laboratory report UCID-21118, 14 August 1987.

7. J. L. Walsh and P. B. Ulrich, "Thermal blooming in the atmosphere", in Laser Beam Propagation in the Atmosphere, J. W. Strohbehn, Ed., Springer-Verlag,

Berlin, 1978.

8. M. Lax, W. H. Louisell and W. B. McKnight, "From Maxwell to paraxial wave optics", Phys. Rev. A11,1365-1370 (1975).
9. A. K. Gautesen and J. R. Morris, "A Geometric optics approximation to a model of phase-compensated whole-beam thermal blooming", Lawrence Livermore National Laboratory report UCID-21501, 12 September 1988
10. J. W. Hardy, "Active optics: a new technology for the control of light", Proc. IEEE 66,651-697 (1978).
11. V. I. Tatarski, Wave Propagation in a Turbulent Medium, R. A. Silverman, trans., McGraw-Hill, New York, 1961.
12. J. W. Goodman, Statistical Optics, ch. 8, John Wiley and Sons, New York, 1985.
13. J. A. Fleck, J. R. Morris and M. D. Feit, "Time dependent propagation of high energy laser beams through the atmosphere", Appl. Phys. 10,129-160 (1976); 14,99-115 (1977).
14. A. S. Monin and A. M. Yaglom, Statistical Fluid Mechanics, Vol. 2, MIT Press, Cambridge 1975.
15. J. A. Viecelli, "Thermal blooming threshold computations with a Markov model of velocity turbulence", Lawrence Livermore National Laboratory report UCID-21589, 30 November 1988.
16. G. E. P. Box and G. M. Jenkins, Time Series Analysis, ch. 3, Holden-Day, San Francisco 1976.
17. R. E. Hufnagel, "Variations of atmospheric turbulence", in Digest of Technical Papers, Topical Meeting on Optical Propagation Through Turbulence (Optical Society of America, Washington, D.C., 1974); G. C. Valley, Appl. Opt. 19, 574-577 (1980).
18. J. Schonfeld, private communication

Figure Captions

1. Linear theory of thermal blooming. The boundary conditions are the field fluctuations **F** at path start and $\mathbf{F^b}$ at path end, and the initial index fluctuation μ^o everywhere along the path. The five Green functions are **J**, $\mathbf{J^b}$, **K**, **L**, **B**. The solution is the field fluctuation **F** at path end and $\mathbf{F^b}$ at path start. The control law **G** relates **F** to $\mathbf{F^b}$.

2. Time evolution of the wave spectrum with turbulence and thermal blooming in a homogeneous medium. There is perfect phase correction at all Fresnel numbers down to $N_{PC} = 10$. Turbulence Fresnel number $N_T = 7.85$.

3. Time evolution of the wave structure function with turbulence and thermal blooming, for the same parameters as Fig. 2.

4. Singularities of the phase correction response kernel M in the complex ν-plane. Mellin transform over the contour $\mathcal{C}$ gives M in the time domain. Singularities in the right half-plane correspond to exponentially growing modes. Singularities in the left half-plane correspond to exponentially damped modes. The accumulation point is an essential singularity corresponding to open-loop growth.

5. Dispersion relation of the most unstable mode in a homogeneous medium. N_P is the Fresnel number of the perturbation which is perfectly phase corrected. The growth rate is normalized to the blooming rate $\dot{N}_\lambda$.

6. Residue denominator of the most unstable mode for perfect phase correction in a homogeneous medium. The value at $N_P \rightarrow \infty$ is $\pi/4$.

7. Propagation factor of the most unstable mode for perfect phase correction in a homogeneous medium.

8. Comparison of theoretical and numerical dispersion relations for a homogeneous medium. Solid line is the analytical calculation, Eq. (16); circles are numerical results of the ORACLE code. Code simulations for many different physical dimensions have been plotted in terms of the dimensionless scaling parameters N_P and $\dot{N}_\lambda$.

9. Comparison of theoretical and numerical spectrum growth in a homogeneous medium excited by an impulse perturbation. Solid line is the analytical calculation, Eq. (54); circles are the ORACLE simulation. The conditions are $N_P = 2$, $\eta_o = 0.1$, and $\Delta N_\lambda = 0.0216$.

10. Turbulence coupling factor of the most unstable mode for perfect phase correction in a homogeneous medium.

11. Exponential part ,Eq. (49), of the spectrum of the most unstable mode in a homogeneous medium, for perfect phase correction of turbulence. The mode amplitude grows exponentially from the initial coupling to the turbulence, Eq. (64).

12. Comparison of the full wave spectrum to the spectrum of the most unstable mode in a homogeneous medium, for perfect phase correction of turbulence at $N_P = 1$ and $N_T = 7.854$. The full spectrum is Eqs. (A9)- (A11); the leading mode spectrum is Eqs. (49) and (64).

13. Dispersion relation of the most unstable mode in a homogeneous medium for various phase correction loop filters. The filter function has the form $g(N_P) = 2^{-(N_{PC}/N_P)^n}$, with $N_{PC} = 4$.

14. Comparison of theoretical and numerical spectra for phase correction of turbulence and thermal blooming. Solid lines are the linearized theory spectra (sum of χ and ϕ variances); symbols are the code spectra (numerical E-field variance). The spectra are labeled with the accumulated OPD from thermal blooming. Phase control gain function is supergaussian with $N_{PC} = 7.85$ and $n = 10$. The atmosphere has uniform absorption, wind speed and turbulence. The simulation is done in the convected frame ($v = 0$). The mesh-filling beam has $N_F = 1000$. The spectra are scaled by $N_T^{5/6}$. Code results are averaged around a circle in κ-space at the indicated radius wavenumber. "Max PCI" indicates the wavenumber with the largest growth rate. (a) $N_T = 4909$, (b) $N_T = 196$, (c) $N_T = 7.85$.

15. Strehl ratio of the ORACLE simulations in Fig. 14.

16. Typical transverse structures produced in numerical simulations of thermal blooming. These plots are from the ORACLE simulation of Fig. 14c at 1.7 waves of blooming. They show the intense beam at the end of the atmospheric path, in the near field. (a) Grey-shade plot of irradiance (dark means high irradiance). (b) Grey-shade plot of phase modulo (2 π) (dark means $+\pi$, light means - π). Cell size $\approx$ phase correction cutoff wavelength.

17. Dispersion relation of the most unstable phase corrected mode for various blooming profiles. The absorbed irradiance decreases exponentially with range along the path, $\Gamma(z) = \Gamma_o \exp(-z/L_a)$. The total length of the path varies from 1 to 7 e-foldings.

18. Damping effect of linear wind shear in a medium with uniform heating. (a) WKB theory dispersion relation of the most unstable phase corrected mode, as a function of the linear shear parameter along the perturbation. (b) Comparison of theoretical and numerical dispersion relations with linear wind shear. Solid lines are slices through the WKB analytical result in (a); circles are ORACLE simulations. (c) Spectrum from ORACLE simulations of uncorrected turbulence in thermal blooming with linear wind shear. Turbulence $N_T = 0.785$. These spectra are time averaged over 4.5 to 9 waves of blooming, and are taken along the axis in κ-space parallel to the direction of linear shear. Squares are S = 0, triangles are S = 0.886, circles are S = 1.77.

19. Effect of linear wind shear on instability growth in an ORACLE simulation of turbulence and blooming. The atmosphere has uniform absorption, wind speed and turbulence, the collimated beam has $N_F = 2000$, the PC control loop has a supergaussian filter with $N_{PC} = 4$ and n = 10, turbulence $N_T = 20$, $\dot{N}_\lambda = 10$ waves/sec, and shear S = 10 along the vertical axis. Pictures are at 2.3 waves of blooming. (a) Grey-shade plot of irradiance at the end of the atmospheric path(dark means high irradiance). Perturbations grow into stripes aligned to the wind shear. (b) Grey-shade plot of far field irradiance in the (κ_x , κ_y) plane. The $\kappa = 0$ boresight is at the center of

the picture. The near field stripes give a diffraction pattern appearance in the far field. Energy is bunched at harmonics of the PC cutoff.

20. Damping effect of random wind shear. The atmosphere has exponentially distributed absorption, Hufnagel-Valley turbulence[17], and a Markovian wind velocity profile with dimensionless shear S. The round collimated beam has $N_F = 4800$, the PC control loop has a supergaussian filter with $N_{PC} = 10$ and $n = 10$, turbulence $N_T = 20$, and $\dot{N}_\lambda = 10$ waves/sec.

21. Perturbation growth below the shear threshold. ORACLE parameters are from Fig. 20, with $S = 1.72$. The spectrum is summed over a ring in the far field at the indicated radius angle.

Figure 1

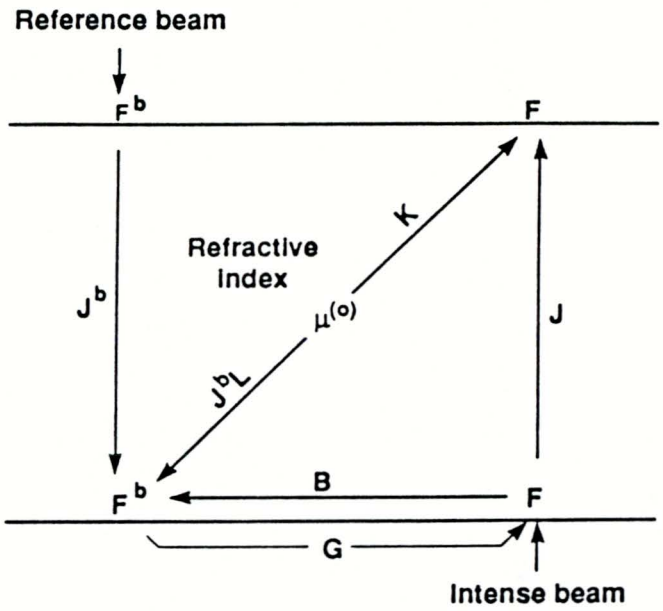

Linear theory of thermal blooming. The boundary conditions are the field fluctuations **F** at path start and $\mathbf{F^b}$ at path end, and the initial index fluctuation μ^0 everywhere along the path. The five Green functions are **J**, $\mathbf{J^b}$, **K**, **L**, **B**. The solution is the field fluctuation **F** at path end and $\mathbf{F^b}$ at path start. The control law **G** relates **F** to $\mathbf{F^b}$.

Figure 2

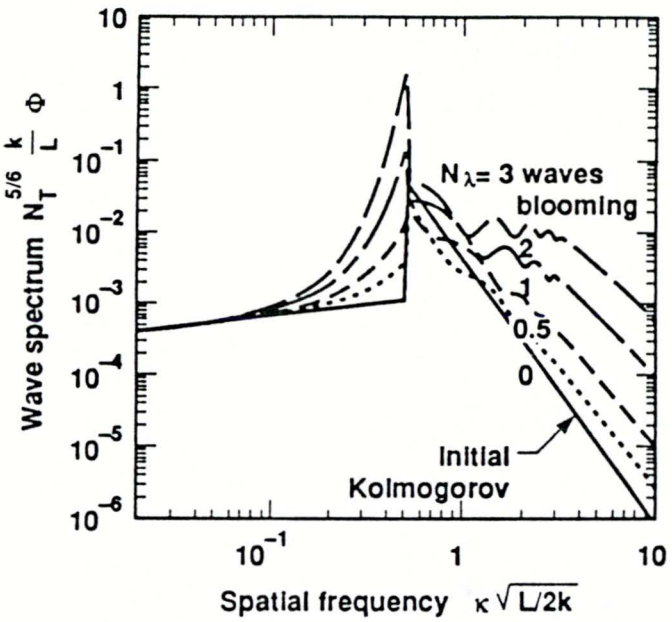

Time evolution of the wave spectrum with turbulence and thermal blooming in a homogeneous medium. There is perfect phase correction at all Fresnel numbers down to $N_{PC} = 10$. Turbulence Fresnel number $N_T = 7.85$.

Figure 3

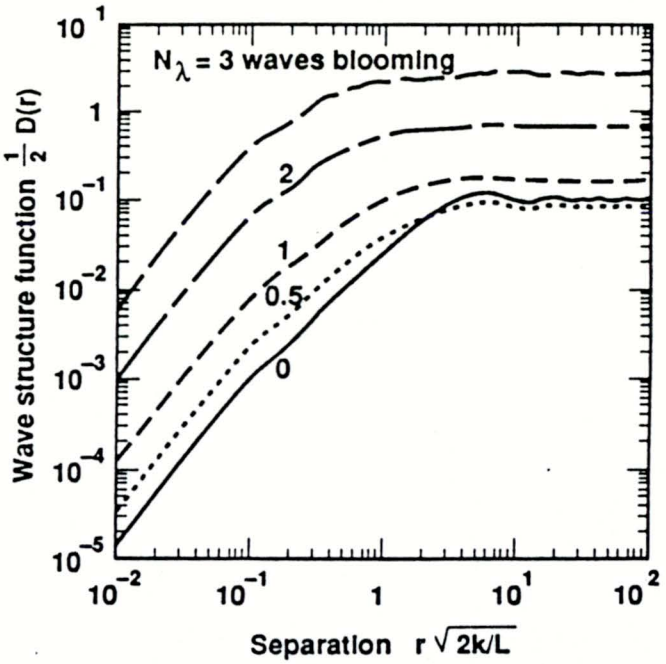

Time evolution of the wave structure function with turbulence and thermal blooming, for the same parameters as Fig. 2.

Figure 4

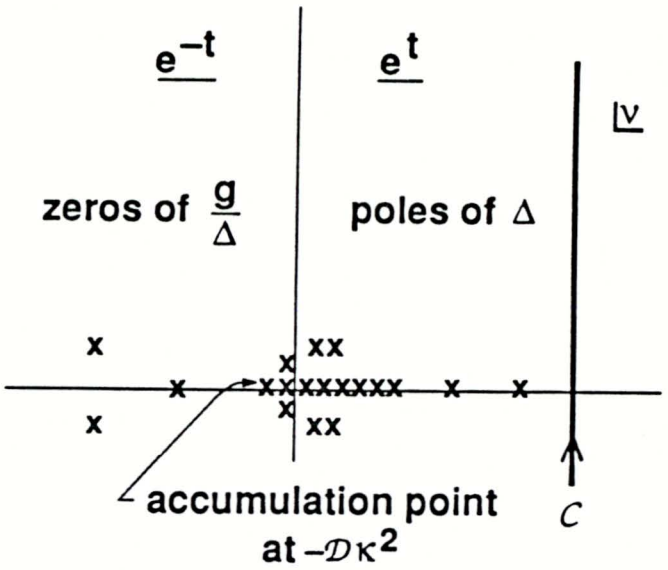

Singularities of the phase correction reponse kernel M in the complex ν-plane. Mellin transform over the contour *C* gives M in the time domain. Singularities in the right half-plane correspond to exponentially growing modes. Singularities in the left half-plane correspond to exponentially damped modes. The accumulation point is an essential singularity corresponding to open-loop growth.

Figure 5a

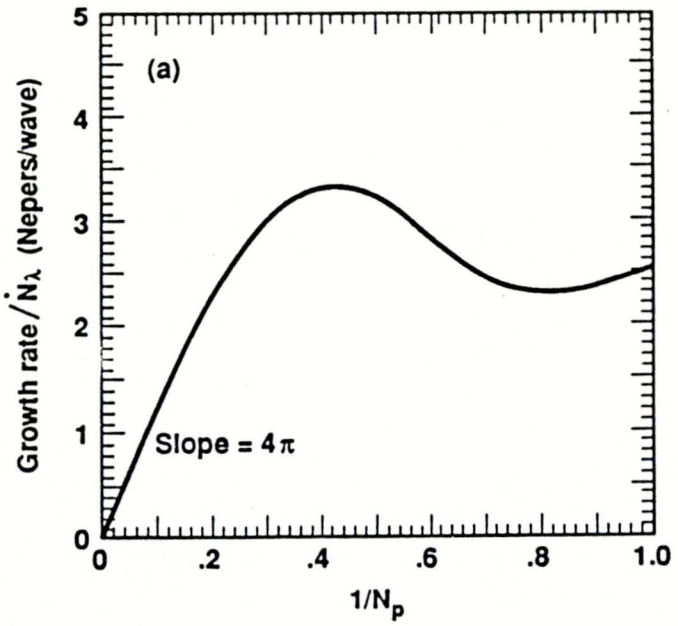

Dispersion relation of the most unstable mode in a homogeneous medium. N_P is the Fresnel number of the perturbation which is perfectly phase corrected. The growth rate is normalized to the blooming rate $\dot{N}_\lambda$.

Figure 5b

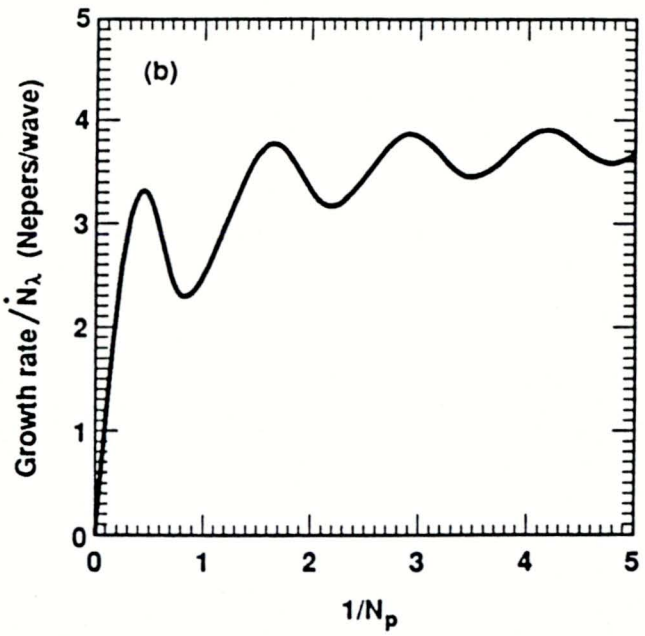

Figure 6

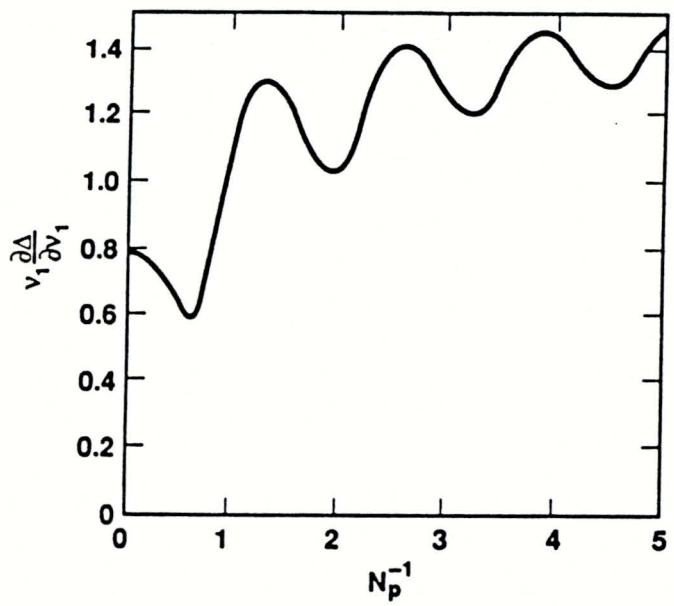

Residue denominator of the most unstable mode for perfect phase correction in a homogeneous medium. The value at N_P --> ∞ is $\pi/4$.

Figure 7a

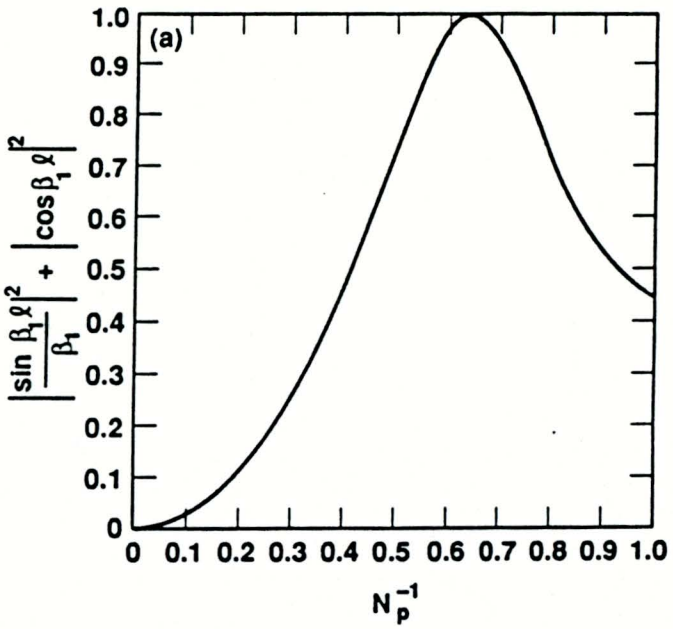

Propagation factor of the most unstable mode for perfect phase correction in a homogeneous medium.

Figure 7b

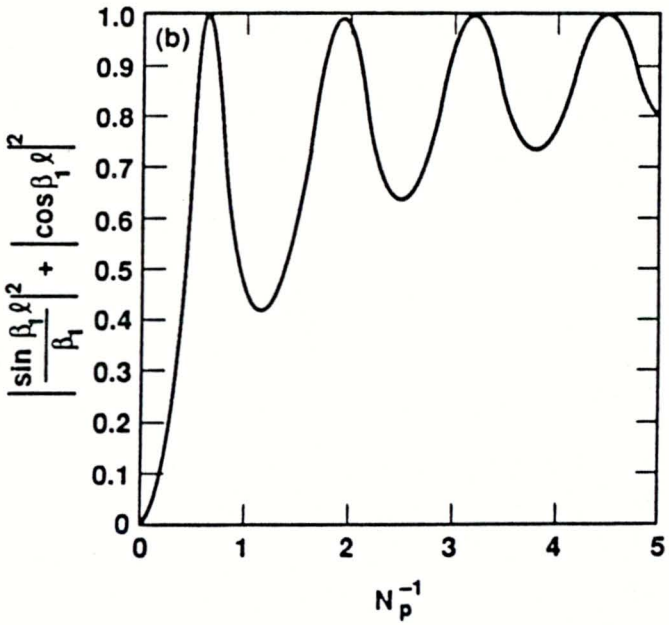
(b)
1.0
0.9
0.8
0.7
0.6
0.5
0.4
0.3
0.2
0.1
0
0
1
2
3
4
5
N_p^{-1}
$\left|\frac{\sin \beta_1 \ell}{\beta_1}\right|^2 + \left|\cos \beta_1 \ell\right|^2$

Figure 8

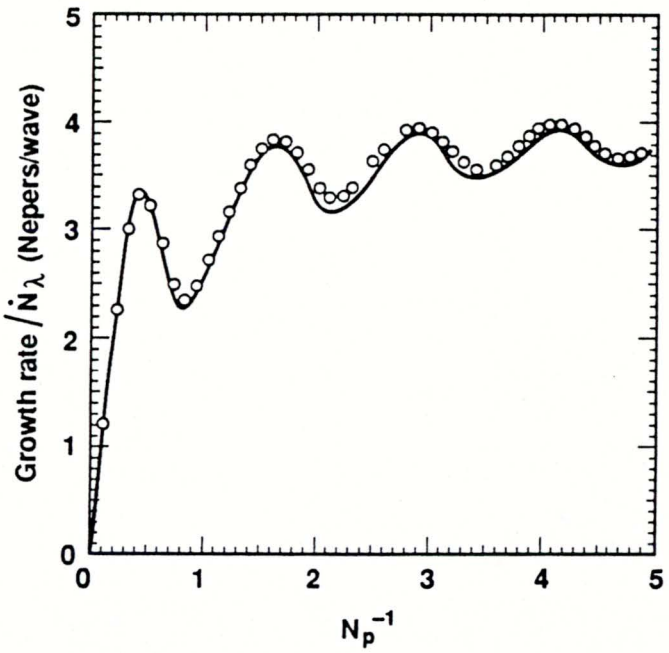

Comparison of theoretical and numerical dispersion relations for a homogeneous medium. Solid line is the analytical calculation, Eq.(16); circles are numerical results of the ORACLE code. Code simulations for many different physical dimensions have ben plotted in terms of the dimensionless scaling parameters N_P and $\dot{N}_\lambda$.

99-00-0289-1439(12)

KAS-OO2-U-3828-FIG2

Figure 9

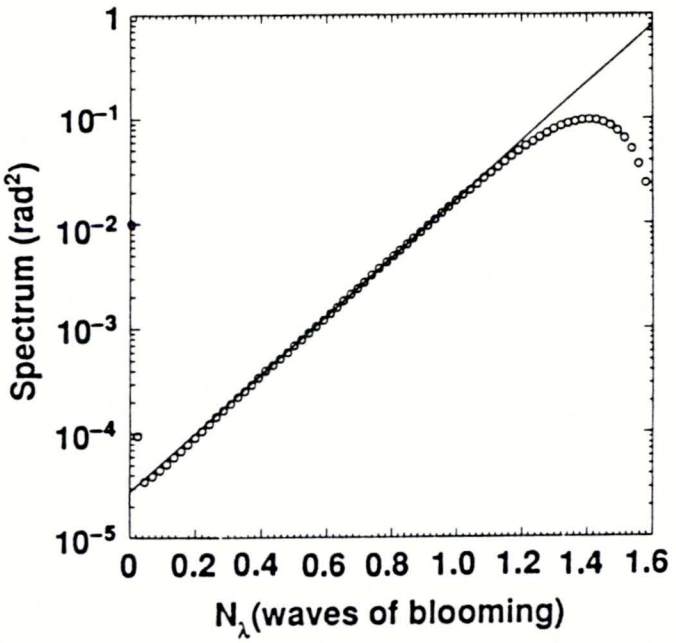

Comparison of theoretical and numerical spectrum growth in a homogeneous medium excited by an impulse perturbation. Solid line is the analytical calculation, Eq.(54); circles are the ORACLE simulation. The conditions are $N_P = 2$, $\eta_0 = 0.1$, and $\Delta N_\lambda = 0.0216$.

Figure 10

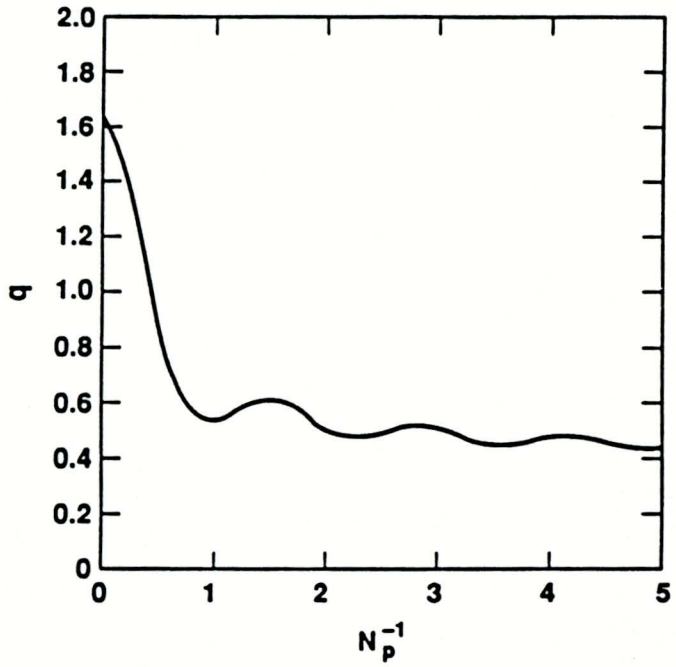

Turbulence coupling factor of the most unstable mode for perfect phase correction in a homogeneous medium.

Figure 11

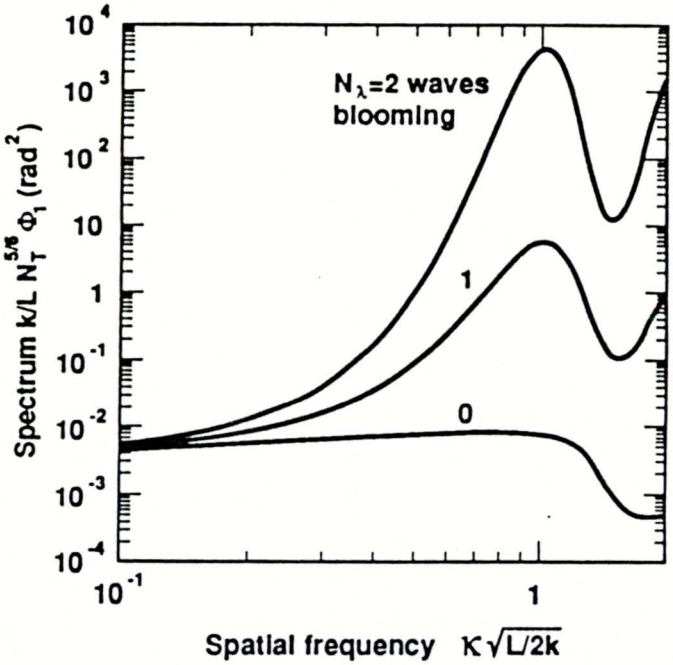

Exponential part Eq.(49) of the spectrum of the most unstable mode in a homogeneous medium, for perfect phase correction of turbulence. The mode amplitude grows exponentially from the initial coupling to the turbulence Eq.(64).

Figure 12

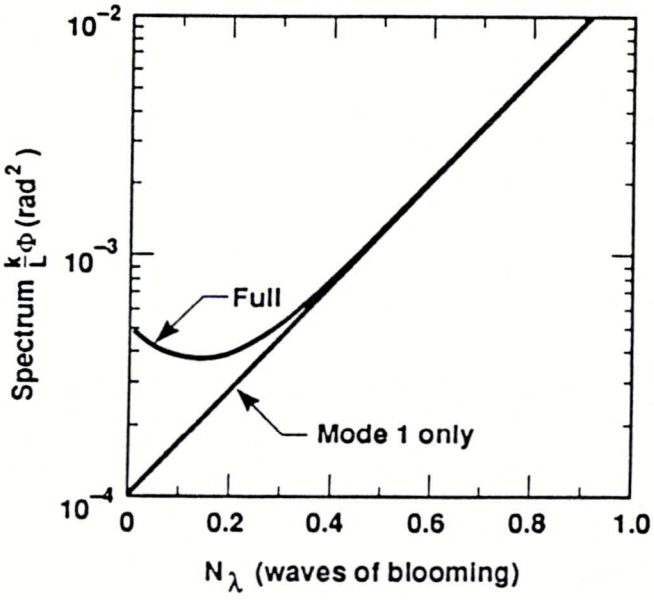

Comparison of the full wave spectrum to the spectrum of the most unstable mode in a homogeneous medium, for perfect phase correction of turbulence at $N_P = 1$ and $N_T = 7.854$. The full spectrum is Eqs.(A9)-(A11); the leading mode spectrum is Eqs.(49) and (64).

Figure 13

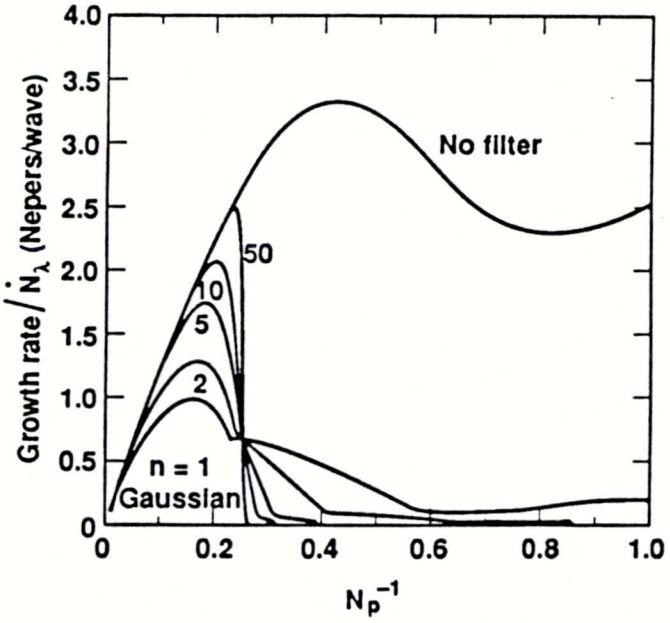

Dispersion relation of the most unstable mode in a homogeneous medium for various phase correction loop filters. The filter function has the form $g(N_P) = 2^{-(N_{PC}/N_P)^n}$, with $N_{PC} = 4$.

Figure 13

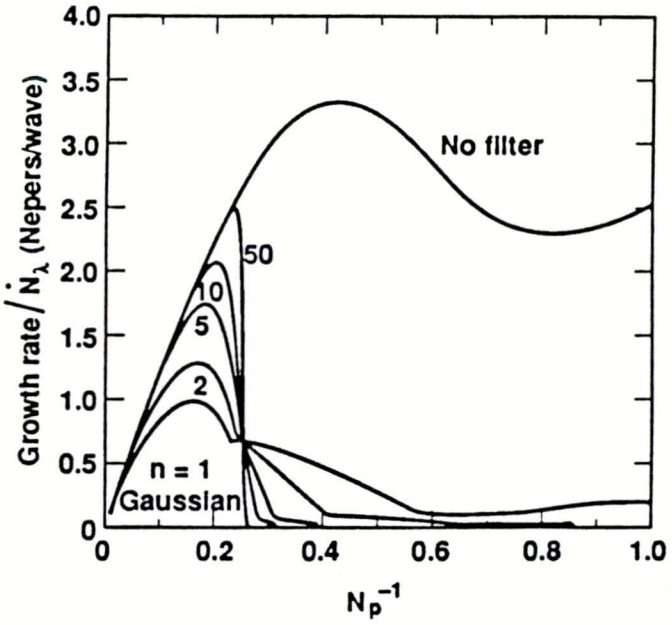

Dispersion relation of the most unstable mode in a homogeneous medium for various phase correction loop filters. The filter function has the form $g(N_P) = 2^{-(N_{PC}/N_P)^n}$, with $N_{PC} = 4$.

Figure 14a

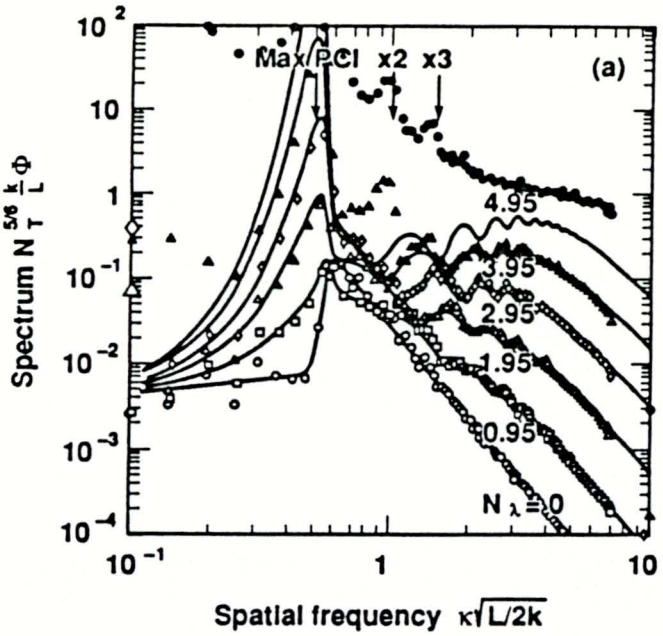

Comparison of theoretical and numerical spectra for phase correction of turbulence and thermal blooming. Phase control filter function is supergaussian with N_{PC} = 7.85 and n = 10. The atmosphere has uniform absorption, wind speed and turbulence . The simulation is done in the convected frame(v = 0). The mesh-filling beam has N_F = 1000. The spectra are scaled by $N_T^{5/6}$. Code results are averaged around a circle in κ-space at the indicated radius wavenumber. "Max PCI" indicates the wavenumber with the largest growth rate.

(a) N_T = 4909

Figure 14b

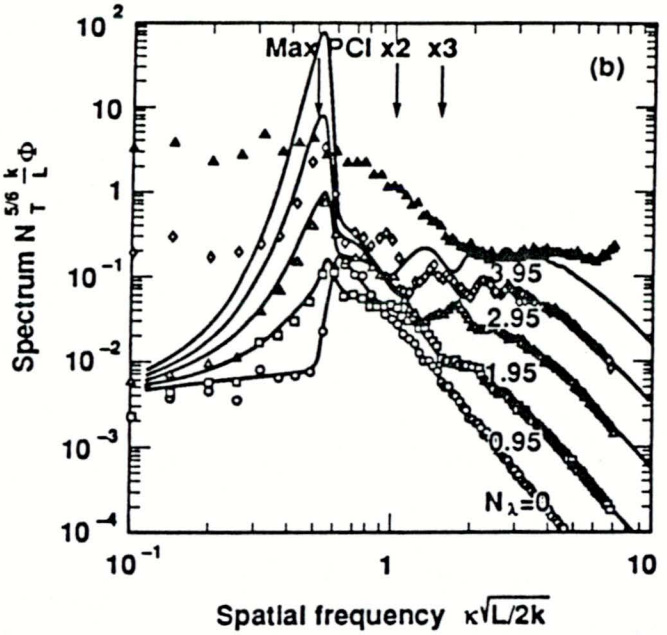

(b) N_T = 196

Figure 14c

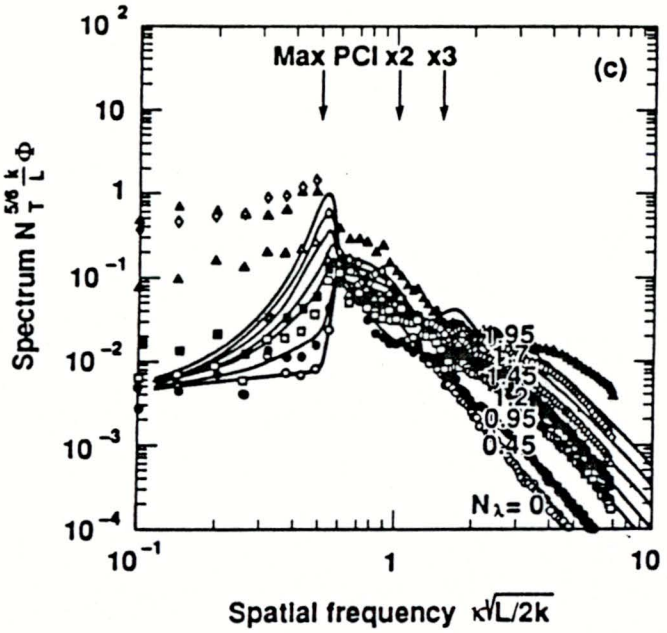

(c) $N_T = 7.85$

Figure 15

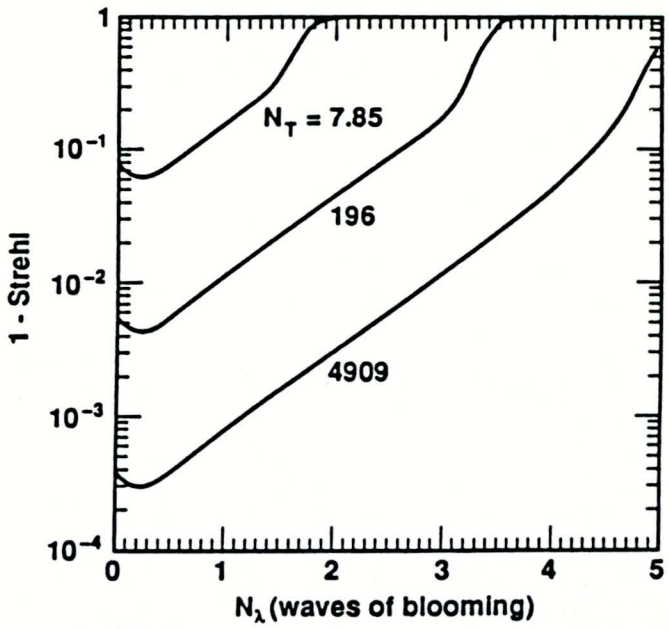

Strehl ratio of the ORACLE simulations in Fig. 14.

Figure 16a

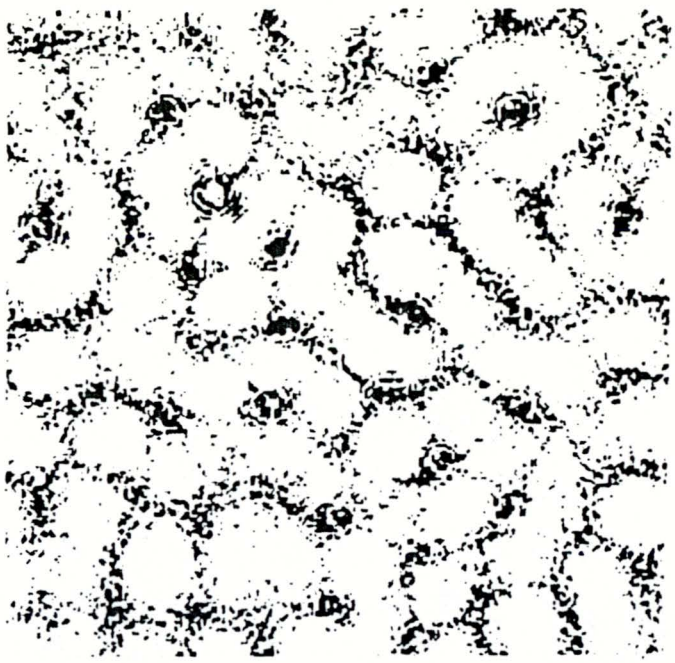

Typical tranverse structures produced in numerical simulations of thermal blooming. These plots are from the ORACLE simulation of Fig. 14c at 1.7 waves of blooming. They show the intense beam at the end of the atmospheric path, in the near field. Cell size ≈ phase correction cutoff wavelength.

(a) Grey-shade plot of irradiance(dark means high irradiance).

Figure 16b

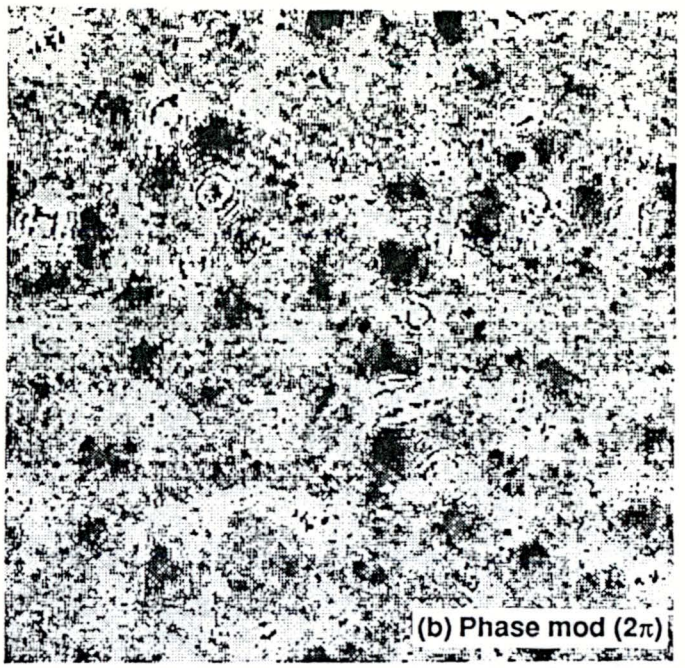

(b) Grey–shade plot of phase modulo (2π) (dark means +π, light means -π).

Figure 17

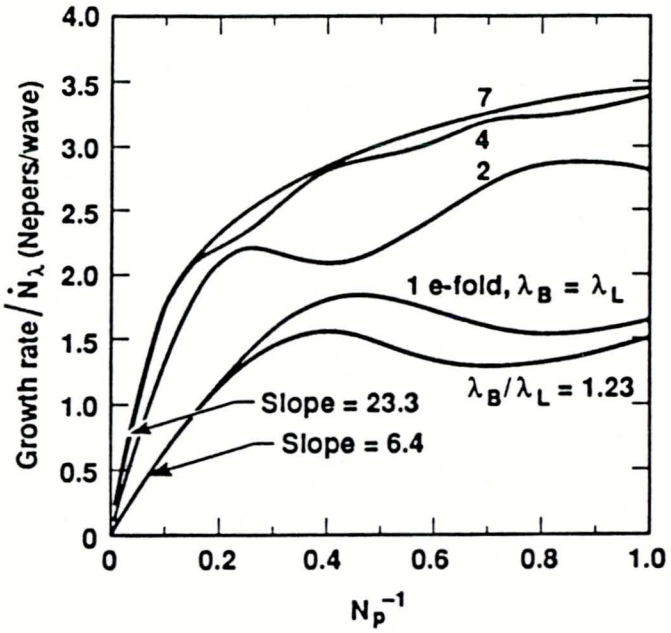

Dispersion relation of the most unstable phase corrected mode for various blooming profiles. The absorbed irradiance decreases exponentially with range along the path, $\Gamma(z) = \Gamma_0 \exp(-z/L_a)$. The total length of the path varies from 1 to 7 e-foldings.

Figure 18a

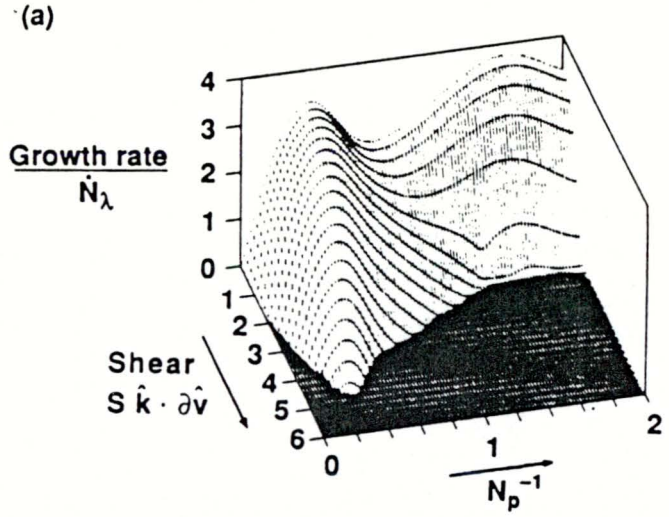

Damping effect of linear wind shear in a medium with uniform heating.
(a) WKB theory dispersion relation of the most unstable phase corrected mode, as a function of the linear shear parameter along the perturbation.

Figure 18b

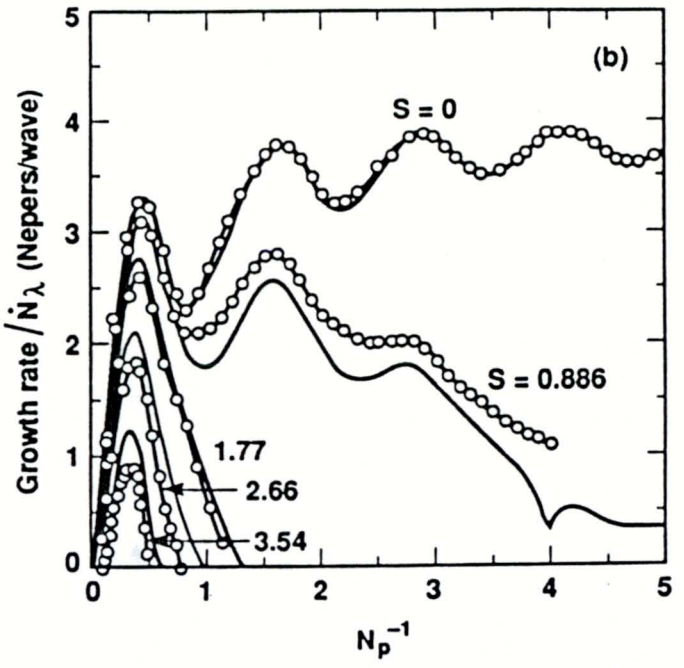

(b) Comparison of theoretical and numerical dispersion relation with linear wind shear. Solid lines are slices through the WKB analytical result in (a); circles are ORACLE simulations.

99-00-0289-1439(15)

KAS-002-U-3828-FIG3

Figure 18c

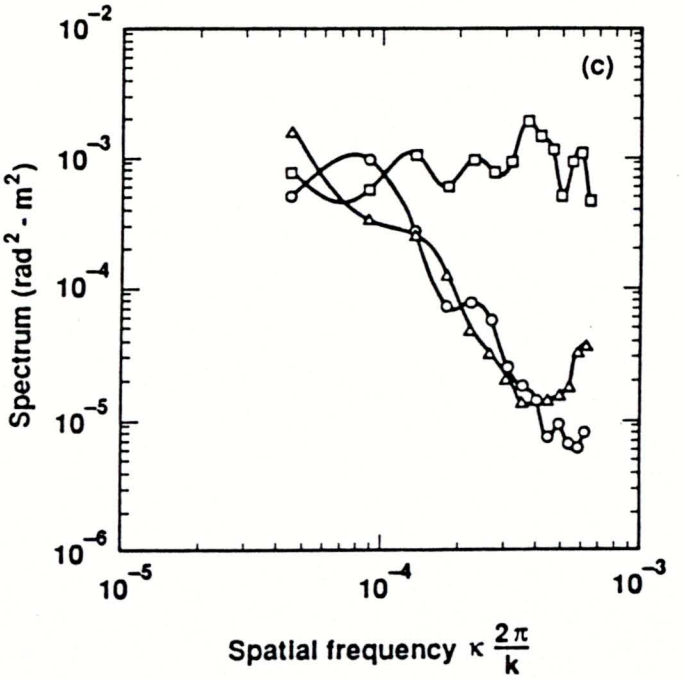

(c) Spectrum from ORACLE simulations of uncorrected turbulence in thermal blooming with linear wind shear. Turbulence N_T = 0.785. These spectra are time averaged over 4.5 to 9 waves of blooming, and are taken along the axis in κ-space parallel to the direction of linear shear. Squares are S = 0, triangles are S = 0.886, circles are S = 1.77.

Figure 19a

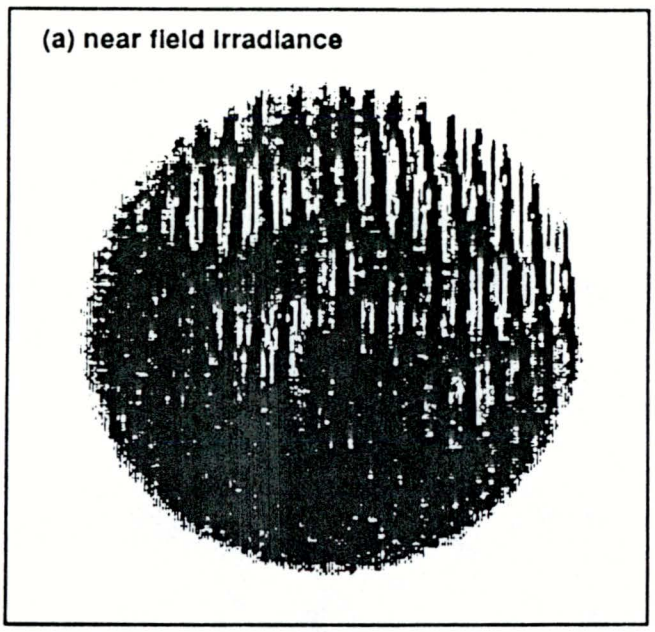

Effect of linear wind shear on instability growth in an ORACLE simulation of turbulence and blooming. The atmosphere has uniform absorption, wind speed and turbulence, the collimated beam has $N_F = 2000$, the PC control loop has a supergaussian filter with $N_{PC} = 4$ and $n = 10$, turbulence $N_T = 20$, $\dot{N}_\lambda = 10$ waves/sec, and shear $S = 10$ along the vertical axis. Pictures are at 2.3 waves of blooming.
(a) Grey-shade plot of irradiance at the end of the atmospheric path(dark means high irradiance). Perturbations grow into stripes aligned to the wind shear.

Figure 19b

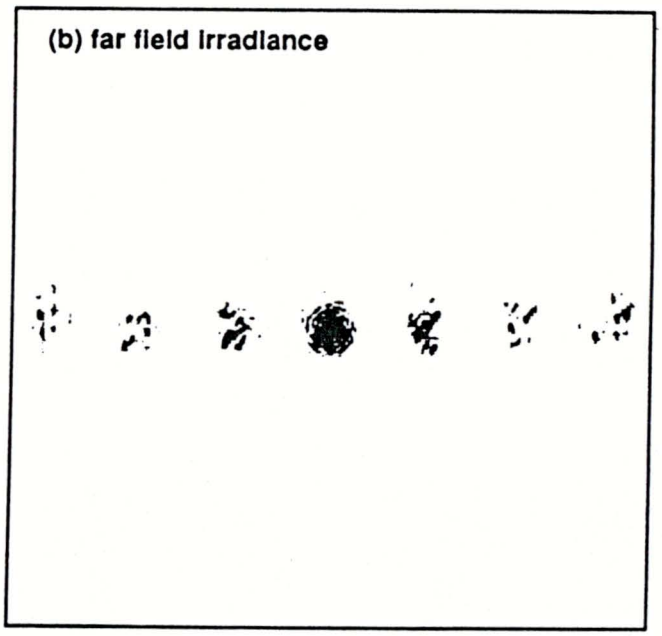

(b) Grey-shade plot of far field irradiance in the (κ_x , κ_y) plane. The $\kappa = 0$ boresight is at the center of the picture. The near field stripes give a diffraction pattern in the far field. Energy is bunched at harmonics of the PC cutoff.

Figure 20

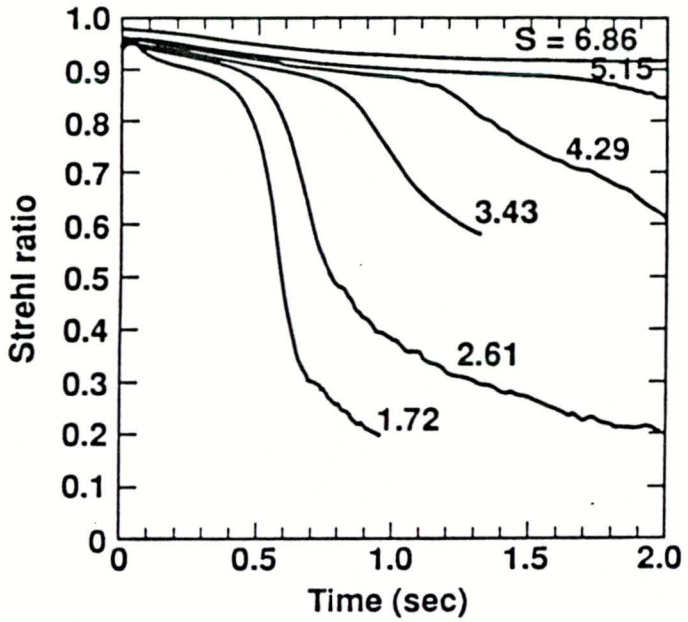

Damping effect of random wind shear. The atmosphere has exponentially distributed absorption, Hufnagel-Valley turbulence[17], and a Markovian wind velocity profile with dimensionless shear S. The round collimated beam has N_F = 4800, the PC control loop has a supergaussian filter with N_{PC} = 10 and n = 10, turbulence N_T = 20, and $\dot{N}_\lambda$ = 10 waves/sec.

Figure 21

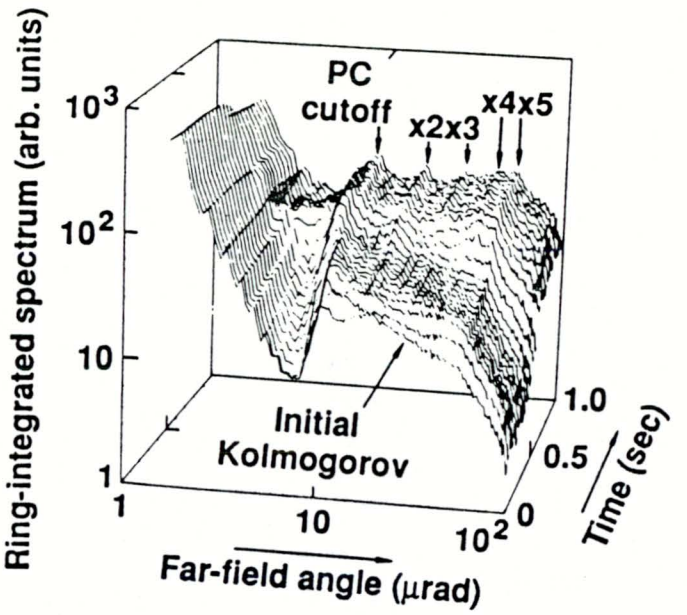

Perturbation growth below the shear threshold. ORACLE parameters are from Fig. 20, with S = 1.72. The spectrum is summed over a ring in the far field at the indicated radius angle.